QUANTUM MECHANICAL TREATMENT OF FULLENE-BASED SYSTEMS DOPED WITH VARIOUS METAL AND NON-METAL ELEMENTS AS PROSPECTIVE SPIN-QUBITS

A THESIS SUBMITTED TO
THE GRADUATE SCHOOL OF NATURAL AND APPLIED SCIENCES
OF
MIDDLE EAST TECHNICAL UNIVERSITY

BY

SERKAN POLAD

IN PARTIAL FULFILLMENT OF THE REQUIREMENTS
FOR
THE DEGREE OF MASTER OF SCIENCE
IN
MICRO AND NANOTECHNOLOGY

JULY 2010

Approval of the thesis:

QUANTUM MECHANICAL TREATMENT OF FULLERENE-BASED SYSTEMS DOPED WITH VARIOUS METAL AND NON-METAL ELEMENTS AS PROSPECTIVE SPIN-QUBITS

Submitted by **SERKAN POLAD** in partial fulfillment of the requirements for the degree of **Master of Science in Micro and Nanotechnology Program, Middle East Technical University** by,

Prof. Dr. Canan Özgen _____
Dean, Graduate School of **Natural and Applied Sciences**

Prof. Dr. Zuhal Küçükyavuz _____
Head of The Program, **Micro and Nanotechnology**

Prof. Dr. Şakir Erkoç _____
Supervisor, **Physics Dept., METU**

Prof. Dr. Işık Önal _____
Co-Supervisor, **Chem.Eng. Dept., METU**

Examining Committee Members:

Prof. Dr. M. Kemal Leblebicioğlu _____
Electrical and Electronics Engineering Dept., METU

Prof. Dr. Şakir Erkoç _____
Physics Dept., METU

Assoc. Prof. Dr. Yusuf İpekoğlu _____
Physics Dept., METU

Assoc. Prof. Dr. Hüseyin Oymak _____
Physics Dept., Atılım University

Assist. Prof. Dr. Hande Toffoli _____
Physics Dept., METU

Date: _____

I hereby declare that all information in this document has been obtained and presented in accordance with academic rules and ethical conduct. I also declare that, as required by these rules and conduct, I have fully cited and referenced all material and results that are not original to this work.

Name, Last name : Serkan Polad

Signature :

ABSTRACT

QUANTUM MECHANICAL TREATMENT OF FULLERENE-BASED SYSTEMS DOPED WITH VARIOUS METAL AND NON-METAL ELEMENTS AS PROSPECTIVE SPIN-QUBITS

Polad, Serkan

M.S., Micro and Nanotechnology Program

Supervisor: Prof. Dr. Şakir Erkoç

Co-Supervisor: Prof. Dr. Işık Önal

July 2010, 87 pages

In this thesis, We have calculated the optimized geometries, electronic structures and spin distributions of metal and non-metal elements Li, Na, N and P doped C_{60} fullerene dimers and trimers with different spin multiplicities using hybrid density functional theory (DFT) at the B3LYP/6-31G level of theory. Natural population analysis and Mulliken population analysis show that non-metal elements (N, P) inside the C_{60} fullerene dimers and trimers are well isolated and preserve their electronic structures while charge transfer processes occur between metal elements(Li, Na) and C_{60} structures. Energy calculations showed that both doped and undoped linear C_{60} structures are energetically lower than triangular C_{60} structures. Calculated spin density distributions make non-metal doped C_{60} structures advantageous over metal doped C_{60} cages as spin cluster qubits.

Keywords: Quantum information, Quantum computation, Fullerenes, Density Functional Theory.

ÖZ

ÇEŞİTLİ METAL VE METAL OLMAYAN ELEMENTLERLE KATKILANDIRILMIŞ FULLEREN-ESASLI YAPILARIN SPİN KÜBİT ÖZELLİKLERİNİN KUANTUM MEKANİĞE GÖRE İNCELENMESİ

Polad, Serkan

Yüksek Lisans, Mikro ve Nanoteknoloji Programı

Tez Yöneticisi: Prof. Dr. Şakir Erkoç

Ortak Tez Yöneticisi: Prof. Dr. Işık Önal

Temmuz 2010, 87 sayfa

Bu tezde, Li, Na, N ve P metal ve metal olmayan elementlerle katkılandırılmış ikili ve üçlü C_{60} fullerenlerin en uygun şekle getirilmiş geometrilerini, elektronik yapılarını ve spin dağılımlarını farklı spin değerleri için yoğunluk fonksiyon teorisi (DFT) metodu B3LYP/6-31G temel seviyesinde hesapladık. Doğal popülasyon ve Mulliken popülasyon analizleri gösterdi ki C_{60} kafes yapıları içerisindeki Li ve Na metal elementleri ve C_{60} kafes yapılar arasında yük transferi olurken, C_{60} kafes yapıları içerisindeki metal olmayan elementler N ve P iyi isole edildiler ve elektronik yapılarını korudular. Enerji hesaplamarı gösterdi ki; katkılandırılmış ve katkılandırılmamış lineer C_{60} yapılar enerji olarak üçgensel C_{60} yapılardan daha düşüktür. Spin dağılımlar gösterdi ki; metal olmayan elementlerle katkılandırılmış C_{60} yapılar spin kübit özellikleri bakımından metal elementlerle katkılandırılmış yapılara göre daha avantajlı durumdadırlar.

Anahtar kelimeler: Kuantum bilgi teorisi, Kuantum bilgisayarlar, Fullerenler, Yoğunluk fonksiyon teorisi.

To the beautiful people who uses not only their minds but also their hearts

ACKNOWLEDGMENTS

I am very thankful to my supervisor Prof. Dr. Şakir Erkoç for his invaluable helps and guidance. In addition, it is a pleasure to pay tribute to my co-supervisor Prof. Dr. Işık Önal for his help on this study. I owe so many things to Mete Özay from METU/Computer Engineering Dept. for his friendship, support and his efforts on supplying computer knowledge. I am so much grateful to Dr. Mehmet Ferdi Fellah from METU/Chemical Engineering Department for his help on Gaussian03 software and for his useful discussions.

I am very thankfull to Ms Ling Ge from the Oxford Materials group for her usefull discussions and suggestions about the subjects that this thesis covers. I especially thank our first assistant in METU/Advanced physics program and a great friend, teacher, writer and beautiful man Dr. Emre Sururi Taşçı, his wife Bengü Yazıcıoğlu Taşçı and their lovely child Ece for their friendship. I would also like to thank my friends from METU Physics Department Şeçkin Kıntaş, Cemal Dursun, S. Eren Özmen, Erhan Akbulut, H. Başar Şık and Yakup Kaya for the friendship and their support.

During the study and preparation my friends İsmail Ayraç, Ünsal Arabacı, Köksal Arabacı, Tolga Ödemiş, Muharrem Ergün, Can Ergün, Raşit Ulusaloğlu, Kubilay Çiftçi and Veysel Arslan from my neigbour in Ankara/Yenimahalle showed great patience and support to me and i would like to thank them for that.

I am especially indebted to my mother and sister for their unstopped support throughout my entire life. I would like to thank my relative Hasan Güvercinci for his way of looking at life, his discussions on quantum physics and time problem. And i am also thankfull to Soren Kierkegaard for his friendship.

Finally, i would like to thank TUBITAK for partial support through the project TBAG-107T142.

TABLE OF CONTENTS

LIST OF TABLES

LIST OF FIGURES

CHAPTER 1

INTRODUCTION

1.1 Nanotechnology

Although the term nanotechnology was first used and defined as the ability to engineer materials precisely at the scale of nanometers in 1974 by N. Taniguchi [1] from University of Tokyo, the birth of nanotechnology is said to have occurred in 1959 at an American Physical Society meeting when R. Feynman gave his speech "There is Plenty of Room at the Bottom" and later he published it as an article [2]. In his speech, he was talking about imagination of new discoveries if we make materials and devices at the atomic and molecular scale. He also stated that a new class of instrumentation is needed to measure and manipulate the properties of nanoscale (10^{-9}-10^{-7} m) structure.

Feynman's talk focused mainly on solid state physics instead of fundamental physics. Because when the size of the structure diminishes to molecular and atomic dimensions, main role of classical physical principles is replaced and emergence of new phenomenons are inevitable such as wave-like transport. At this level of sizes, classical approximations that treat electrons as particles are not proper any more and these systems satisfy the law of quantum mechanics since the wave character of electrons becomes more pronounced .

Consider a school bus, when its size is reduced to nanoscale, problems with the friction will disappear. Mass and inertia become irrelevant due to the reduced size but there will be problems related to the electric and magnetic properties. Also there will be changes when we reduce the size of a big gold piece to the nanoscale; the gold's color, melting point and chemical properties will change. To understand why this happens,

nanotechnology uses the benefits from many disciplines. Physicists care about the properties of matters, chemists are generally concerned about molecules and engineers are concerned with the understanding and utilization of nanoscale materials.

In 1980s, instruments were invented as a result of Feynman's ideas. These instruments, including scanning tunneling microscopes and atomic force microscopes, have become important research tools. Today a large number of nanoparticle based materials such as paints nano particle-doped materials, sunscreens and nano-enhanced golf and tennis balls are used.

If we become more futuristic, we can say that nanotechnology will have an strong effect on military and other industries. Effect of nanotechnology on military applications is increasing and has a huge impact on it, usage of nanorobotics, nanoelectronics and nanobased armors and special nanobio devices will be realistic in the coming years. Table 1 shows the potential and future markets for nanotechnology.

Nano related materials and sevices could be a $1 trillion market by 2015 and increasing approximately ten percent each year according to U.S National Science and Foundation's predictions [4-8]. Nanotechnology is already a priority to goverments and technology companies in the world; their research capabilities and expenses are growing each year.

The results of this growth can be understood from the patent activities, Table 2 shows the patent activities of U.S. The number of total of patents referencing the word "nano" is 21122 and there are 41,208 pending U.S. Patent Applications that reference only nano [9] in 2009. Therefore it seems that nanotechnology is one of the fastest growing industries.

Table 1**:** Potential and future markets for nanotechnology [3].

	Current	1-5 years	6-10 years	10-50 years
Health care/Medicine	Sun screens	Biological nano sensors for diagnostics	Artificial muscle lab on a chip technology for more efficient drug and gene delivery	Nano machines for in vivo treatment Nanopumps/valves for tissue engineering /artificial organs
Energy	Nano-catalyst enhanced fuels for better efficiency	Nanomaterials for fuel cells/batteries	More efficient solar cells using nanotechnology	Nanomaterials for hydrogen storage fuell cells
Security		Nano bar coding and tagging Nanotubes for thermal protection		
Electronics			Carbon nanotube electronic components	Nanomaterials in light emiting diodes and PV devices Single electron/ molecule devices
Communications/ computation			Flat panel flexible displays using nanotechnology High density data storage using nano magnetic effects	Faster processing using quantum computing DNA computers

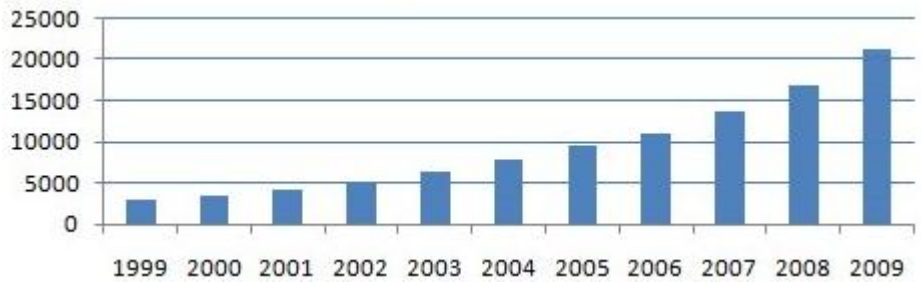

Figure 1: Cumulative total number of U.S patents referencing nano [9].

1.2 Orbital Hybridization and New Carbon Materials

This subsection is mainly based on Refs [10].

Usage of carbon based materials has a huge impact on the development of nanotechnology and it served as one of the most important factors that increased the popularity of nanotechnology. Even though carbon is the sixth most common element in the universe, it is the defining factor for the microscopic act of life. The reason for this probably that carbon binds itself to other light atoms without large expense of energy. Furthermore, carbon based materials have a great affect on nanotechnological applications because of their unique structural, electrical, magnetic and thermal properties caused by the ability of forming possible hybridized orbitals.

A carbon material can be found in many different forms such as graphene, diamond, carbon nanotube and fullerene. Main reason for this variety is the orbital hybridization that is also responsible for the unique character of these clusters.

Electronic configuration of carbon is $\mathbf{1s^2 2s^2 2p^2}$ containing six electrons and four electrons in the $\mathbf{2s^2 2p^2}$ orbitals are called valence electrons. Hybridizations occur when s and p orbitals in the **n=2** shell make a linear combination. Three possible hybridisation occurs in carbon materials: **sp**, $\mathbf{sp^2}$ and $\mathbf{sp^3}$; other elements such as Ge shows $\mathbf{sp^3}$

hybridization and lack of **sp** and **sp^2** hybridization could be related to the lack of Ge based organic materials. In order to clarify the hybridisation of orbitals we discuss in detail **sp** hybridization;

sp hybridization is a combination of 2s and one of the 2p orbitals out of **2p$_x$** and **2p$_y$**. We represent the hybridized wave function as;

$$|sp_1\rangle = a_1|2s\rangle + a_2|2p_x\rangle \quad (1.1)$$

$$|sp_2\rangle = a_3|2s\rangle + a_4|2p_x\rangle \quad (1.2)$$

or

$$|sp_1\rangle = b_1|2s\rangle + b_2|2p_y\rangle \quad (1.3)$$

$$|sp_2\rangle = b_3|2s\rangle + b_4|2p_y\rangle \quad (1.4)$$

Using the orthonormality condition we can find a_n or b_n values and write wavefunctions once more;

$$|sp_1\rangle = \frac{1}{\sqrt{2}}(|2s\rangle + |2p_x\rangle \quad (1.5)$$

$$|sp_2\rangle = \frac{1}{\sqrt{2}}(|2s\rangle - |2p_x\rangle \quad (1.6)$$

Positive and negative signs mean that binding energy will be higher in the +x direction for **sp$_1$** and –x direction for **sp$_2$**. Figure 2 illustrates the overlap or the orbitals for this **sp** hybridization.

Similarly, in sp^2 hybidization; 2s and two 2p orbitals are hybirized and in sp^3 hybidization; 2s orbital and three 2p orbitals are mixed with each other to form sp^3 hybidization.

Carbon exists in two main forms, diamond graphene with **sp^3** and **sp^2** orbital hybridization. Discovery of carbon nanotube [13] and C_{60} fullerene [14] also known as buckminsterfullerene created a bridge between different disciplines because of different

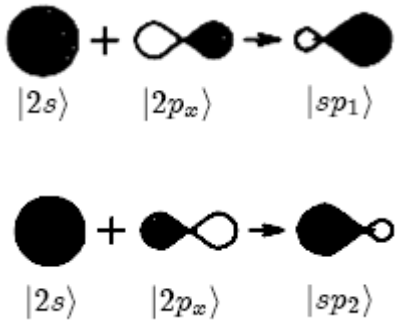

Figure 2: Orbitals for the **sp** hybridization [12].

technological applications. For example today there are numerous experimental and theoretical studies about doped carbon and other type of fullerenes and nanotubes [15-17], even about fullerene inside nanotubes so-called pepods [19,20]. As shown in Figure 3, special carbon materials like C_{60} fullerenes, carbon nanotubes, graphenes and diamond have different hybridization therefore shows different structural and electrical character.

Table 2: Schematic classification of the different forms of carbon (adapted from [21]).

Form	**C_{60} fullerene**	**Carbon nanotube**	**Graphite**	**Diamond**
Hybridization	Sp^2	Sp^2-sp	Sp^2	Sp^3
Bond length (A^0)	1.40 (C=C) 1.46 (C-C)	1.33-1.44 (C=C)	1.42(C=C)	1.54 (C-C)
Electronic properties	Semiconductor	Metal or Semiconductor	Semi metal	Insulating

Hybridization of s and p orbitals leads either σ-type or π-type covalent chemical bonds and while simple bonding allows us to indicate thermal, structural and mechanical properties, the existence of π orbitals will be essential for electronic and magnetic properties.

Orbital hybridization also occurs in other type of materials such as boron, zinc oxide, gallium nitride, boron nitride, silicon carbide nanotubes and fullerenes etc. and so it is responsible for the different effects shown by these structures in technological applications.

1.3 Birth Of Quantum Computing and Quantum Cryptography

1.3.1 Electronic Technology and Moore's Law

Today we are experiencing the fast growth of electronic devices, silicon based chips take place in every technological application including CD players, cars, televisions and cellular phones etc. This revolution is started with the foundation of integrated circuit by Jack Kilby of Texas Instruments in 1958 for which he received Nobel price in Physics in 2000 [22].

Main speciality of the silicon revolution is the miniaturization of transistors inside the integrated circuits because of enhanced performance and reduced costs. There is a huge growth of the size miniaturization and it is continuing almost exponentially even that the feature size of newest generation silicon devices is 40-45 nm in other words this kind of integrated circuits contain billions of transistors.

In 1965, Gordon Moore, co-founder of Intel , made an empirical prediction, so-called Moore's law, that number of transistors on a microprocessor doubles every 18 to 24 months [23]. This means that fast miniaturization reaches transistors take silicon electronics into the size of the atoms or nanometer scales.

The question is why does the Moore's law seem important and contain essential consequences for today's and future technological applications. Moore's law is

important because when the miniaturization comes to the atomic/molecular scale, processors start being affected by the rules of Quantum Mechanics. For example, thickness of the silicon dioxide used as an insulator for gate electrode in field effect transistors, FET, will be smaller when we reduce the dimensions. If this thickness comes to nanometer scales, electrons leak through by the quantum tunneling effect.

Emergence of quantum mechanical rules in nanometer scale is not the only reason for a new technology. Today's large supercomputers used in scientific research, military, technological applications and film industry waste too much energy both for cooling and running. As an example; TÜBİTAK/ULAKBIM Trgrid project has its supercomputing power of almost 2000 nodes using grid computing in order to provide computational simulation projects running by the researchers in Turkey which is also the main source of computational power of the quantum mechanical calculations of molecules that we made in these thesis studies. The structure of the system distributed to ten locations in Turkey and each refrigerator sized supercomputer in these locations need to be cooled by very big special air conditioning units and waste thousands of kilowatts of power with hundrends of data traffic routers and kilometers of cables. Ulakbim allowed to spent 3 million TL in order to make improvements on the system each year . Even bigger systems are already available in the world located in large cities and getting bigger every year. Finally, the necessity of new technologies operated by physics of quantum mechanics with smaller energy costs will be inevitable in the future.

1.3.2 Feynman's Contribution

Richard Feynman was the first physicist to make most essential contribution to the quantum mechanical way of computation through his famous articles in 1982 [24] and 1985 [25]. The idea of Feynman is an imagination of a computer that could act as a quantum mechanical simulator by using quantum mechanical rules such as superposition. He also made descriptions of the quantum computers in his article in 1982, "Simulating Physics with Computers" by mentioning "quantum computers" and "universal quantum simulators". In his further paper "Quantum Mechanical Computers",

his main goal is to understand how quantum systems could simulate ordinary computers by giving detailed suggestions for quantum implementations of classical tasks.

1.3.3 Quantum Money

The most important idea that made quantum cryptography possible was given by Stephen Wiesner in his article "Conjugate Coding" in late 1960s and his idea is based on the impossibility of counterfeiting a **quantum money** [26].

Unlike classical states quantum states cannot in general be copied because a general quantum system is disturbed by measurement i.e. loses its coherence and yields incomplete information about its state before the measurement, it is the so called no-cloning theorem caused by uncertainty principle and states that we can not copy an unknown state. If we would do it, this is against Heisenberg's uncertainty principle. We can not copy a state with exactly same momentum and position. This un-clonability of quantum states create the idea of quantum money and quantum communication systems in which any outside attempt on a quantum communication channel causes an unavoidable disturbance, alerting the users.

Briefly, Weisner's idea of quantum money is that a central bank can make and verify banknotes but it is impossible for anyone to copy it. By printing random polarized photons on the money the bank will be able to prevent counterfeit, in other words, it is not possible to copy the banknotes since the measurement on the arbitrary quantum states will disturbs it, however, the bank must keep the record of photon polarizations for each banknote. If the bank knows each the quantum states of banknotes, it can find the possibility of a banknote to become a copy.

Taking Weisner's idea as the starting point, the first quantum cryptography protocol, BB84, is published by C. H. Bennett and G. Brassard in 1984 [27]. Since then, lots of quantum cryptography protocols is studied, published and experimentally verified such as A. Ekert's E91 EPR [28], COW coherent one way protocol [29], DPS differential phase shift [30] and S09 Protocol with Private-Public Key [31].

1.3.4 Quantum Algorithms

The structure of the algorithms in any quantum computer can make important improvements on speed up as well as the ones caused by the speciality of quantum hardwares which work based on the principles of quantum mechanics.

The first essential contribution to the idea of quantum computers after R. P. Feynman was proposed by D. Deutsch in 1985 [32] by introducing his "Deutsch Algorithm" and it exhibits two to one speed up over classical ones. In 1992, this algorithm was generalized as Deutsch–Jozsa Algorithm [33] but unfortunately this is not an efficient quantum algorithm because it has not much application and there are classical algorithms that solve that problem efficiently.

Biggest achievement of quantum algorithms is given by Peter Shor's factorization algorithm called Shor's algorithm in 1994 [34]. This algorithm makes possible the factorization of large integers quickly. Besides it is better than the best known classical algorithm. Figure 3 shows the advantage of Shor's algorithm over classical ones. This algorithm was tested experimentally in 2001 by the joint researchers from Stanford University and IBM Almaden Research Center [35]. They were successful in factorization of $N = 15$.

There are other types of theoretically successful algorithms like Grover's search algorithm[36] and Simon's algorithm [37] but none of them could achieve the power of Shor's algorithm.

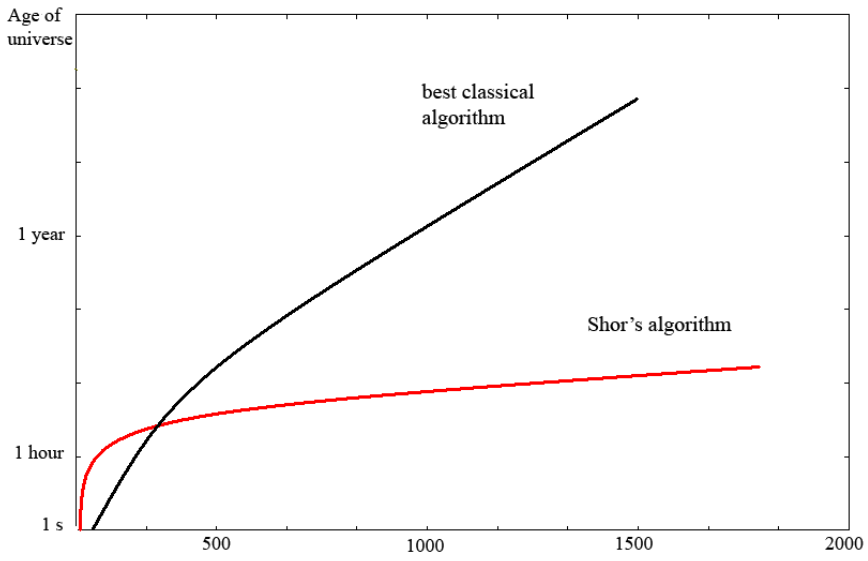

Figure 3: Shor's factorization algorithm vs. best known classical algorithm.

1.3.5 Recent Achievements

Today many applications of quantum information theory are carried out by governments, institutions, and large companies like IBM, France Telecom, Hitachi, Pirelli, Hewlett-Packard and European Space Agency (ESA) etc. Most interesting and striking of all is that D-Wave Inc. in February 13th 2007 announced a 16-qubit quantum computer called ORION [38]. As a first demonstration, ORION solved the Sudoku puzzle. The company has produced 128 qubit quantum computer chip in 2009 [39].

In October 11, 2007 Switzerland used technology of quantum cryptography in collaboration with university of Geneva and the company called id-Quantique to protect voting ballots cast in the Geneva / Switzerland during parliamentary elections and they used more improved technology during the 2008 and 2009 elections, this was the first time to use this technology for this kind of purposes. Japan, Italy, Austria, Spain,

Germany and UK are already testing satellite and ground based quantum communications [40-48].

Recently in 2010, scientists of Harvard University and the University of Queensland, Australia have built a quantum computer and a special algorithm to simulate the Hydrogen molecule [49]. This was the the first quantum computer to simulate and calculate the behavior of a molecule.

1.3.6 Outline

This thesis is divided into seven parts, chapter 2 contains a very introductory descpription of quantum computers and properties of qubits and quantum algorithms. Theoretical background information on quantum chemistry methods used in this thesis is given in chapter 3 including density functional and Hartree Fock methods. In chapter 4, density functional theory results of electronic and geometrical structures of endohedral fullerenes $Li@C_{60}$, $Na@C_{60}$, $N@C_{60}$ and $P@C_{60}$ is given. Chapter 5 contains again results of DFT calculations on metal atoms Li,Na and non-metal atoms N,P doped C_{60} dimer structures. Chapter 6 is divided into two parts, first part have the DFT resılts of electronic and geometrical results of Li, Na, N, P doped linearly [2+2] type aligned three C_{60} fullerene structure while second part contains DFT results of Li, Na, N, P doped [5+5] type aligned triangular C_{60} fullerene structure. Chapter 7 is the conclusion part, this parts compares the spin-qubit properties of structures given in chapters 4-5-6 and possibility of their usage as spin cluster qubits.

CHAPTER 2

QUANTUM WAY OF COMPUTATION

The aim of this chapter is to give a very introductory information about how a quantum computer works and necessary requirements for molecular based quantum computers. This chapter's information is mainly based on the studies in Refs. [50-77] and information inside them constructed the structure of this chapter.

2.1 Quantum Mechanical Tools

2.1.1 Superposition Principle & The Measurement Problem

Schrödinger's equation in quantum mechanics gives how a quantum state evolves in time and it is a linear differencial equation;

$$i\hbar \frac{\partial \psi_{(x,t)}}{\partial t} = \frac{-\hbar^2}{2m} \frac{\partial^2 \psi_{(x,t)}}{\partial x^2} + V(x)\, \psi_{(x,t)} \qquad (2.1)$$

If ψ_1 and ψ_2 are two solutions of this equation then $\psi_1 + \psi_2$ is also the solution of the equation. This property is supported by the linearity of Hilbert space in which wave functions are represented by vectors. Vectors $|\psi_1\rangle$ and $|\psi_2\rangle$ represent states in Hilbert space but a linear combination of these states, $a|\psi_1\rangle + b|\psi_2\rangle$, also represent a state.

This is called the ***superposition principle***. Here $|a|^2$ and $|b|^2$ are probabilities and $|a|^2 + |b|^2 = 1$ from the normalization.

To give a physical example, as we can see from the Figure we can assign $|\psi_1\rangle$ as an electron's ground state and $|\psi_2\rangle$ as its exited state or $|\psi_1\rangle$ for spin up and $|\psi_2\rangle$ for spin down state. However, according to the superposition principle state of electron is in a linear combination of these states. Above a and b coefficients can be arbitrary complex numbers, only requirement is to satisfy the normalization condition i.e. their squares add up to 1. For example, superposition state can be $\frac{1}{\sqrt{5}}|\psi_1\rangle + \frac{2i}{\sqrt{5}}|\psi_2\rangle$ or $\frac{1}{\sqrt{2}}|\psi_1\rangle + \frac{1}{\sqrt{2}}|\psi_2\rangle$.

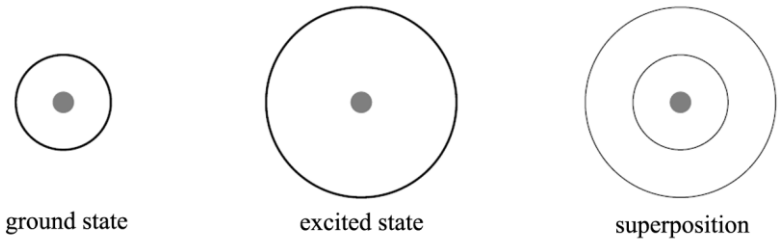

Figure 4: Electron states as a physical example of a superposition state.

This kind of states can be observed experimentally such as effect of interference. In contrast, in classical (macroscopic) world, we are not able to see such states. For example, A car is never in a state of being in our garage and on the top of a tree, simultaneously. The question is why is a superposition of macroscopic states never observed? Problem arised by the behavior of large systems to show classical properties is called ***the measurement problem.*** This phenomenon is very important for all quantum

computer proposals because it is crucial that quantum computer must be well isolated from the environment.

There are many studies including wavefunction collapse mechanisms to try to explain the measurement problem. One of them is given in 2.1.3 and investigates the decoherence phenomenon in the quantum physics.

2.1.2 Quantum Entanglement

Entanglement phenomenon is very crucial not only for quantum cryptography but also for the theory of quantum computing because every proposal of quantum computer gains its power from entanglement as well as quantum paralelism.

We can write two quantum states in their superposition forms as follows;

$$|\psi_1\rangle = \sum_i c_i \, |i\rangle_1 \tag{2.2}$$

$$|\psi_2\rangle = \sum_j d_j \, |j\rangle_2 \tag{2.3}$$

Where $|i\rangle_1$ and $|j\rangle_2$ are basis vectors in Hilbert spaces H_1 and H_2, respectively. Combined system's state is written as;

$$|\psi_1\rangle \otimes |\psi_2\rangle = \left(\sum_i c_i \, |i\rangle_1\right) \otimes \left(\sum_j d_j \, |j\rangle_2\right) = \sum_{ij} \lambda_{ij} \, |i\rangle_1 |j\rangle_2 \tag{2.4}$$

if $\lambda_{ij} = c_i d_j$, it means the state is separable, however $\lambda_{ij} \neq c_i d_j$ then it is said to be non-separable i.e. combined system's state can no longer be expressed as a product state because of this inseparability and such states are called entangled states.

Most famous example of an entangled state is Einstein, Podolsky and Rosen (EPR) state[78] of combined systems A and B;

$$|\Psi\rangle = \frac{1}{\sqrt{2}}(|0\rangle_A |0\rangle_B + |1\rangle_A |1\rangle_B) \tag{2.5}$$

Let's assume that these two systems are away from each other, A is in Turkey and B is in Germany. When we measure A the result is $|0\rangle_A$ with ½ probability and $|1\rangle_A$ with ½ probability and systems state changes (or collapses) to $|0\rangle_A |0\rangle_B$ and $|1\rangle_A |1\rangle_B$ for two different cases, respectively. Therefore after the measurement of A, we measure B in the

Germany and if measured A value is $|0\rangle_A$ we find $|0\rangle_B$ with probability 1 and if measured value of A is $|1\rangle_A$, we find $|1\rangle_B$ with probability 1 after the measurement of B.

Entanglement plays an important role in both explaining the measurement problem and in quantum algorithms.

2.1.3 Decoherence Interpretation

Decoherence program carries great potential to describe the measurement problem and its description has great influence on molecular quantum computer architectures. Decoherence can be known as one of the interpretations of quantum physics by introducing the so-called wave function collapse as a result of the interaction between the environment and the physical system.

The most widely accepted intepretation of quantum mechanics is the Copenhagen interpretation which is based mainly on the studies of Bohr and partly Heisenberg. It contains two important principles making it a non-deteministic interpretation; Bohr's ***complementarity*** and Heisenberg's ***uncertainty*** principles. According to the complementarity principle an object such as an electron can not behave as particle and wave at the same time, while Heisenberg's uncertainty principle makes impossible to determine all the properties at the same time, like energy and time or position and momentum, and we must describe them as probabilities.

Copenhagen interpretation explains the measurement problem as wave function collapses due to the measurement but measurement is not clearly defined in this interpretation in other words, measurement is considered classically.

Decoherence interpretation [63-77], however, tries to explain the measurement problem by giving the idea that correlations between environment (or measurement apparatus) and the system can lead to non-local entanglements which are responsible for the emergence of classicality (measurement problem).

Before giving a mathematical explanation of the wave function collapse caused by the entanglement in decoherence program let's talk about interference loss in the Mach-Zehnder interferometer;

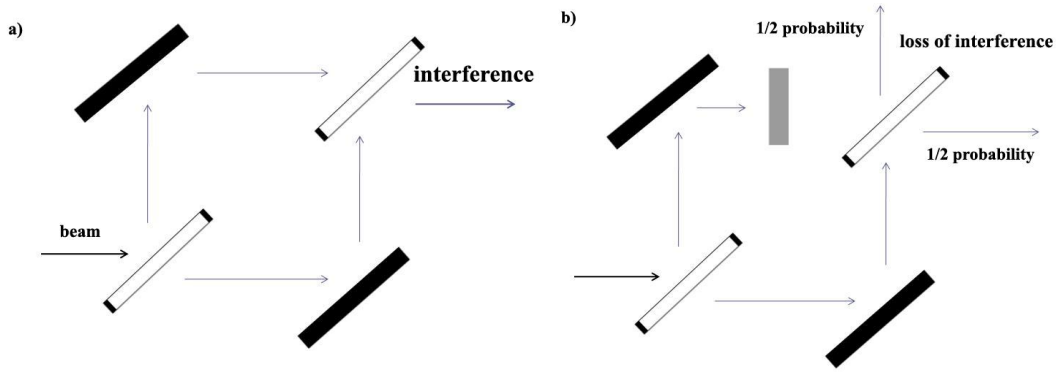

Figure 5**:** Experimental setup to explain the loss of interference.

When we send a photon toward a beam splitter (or a half-silvered mirror), photon will travel in both direction and with the help of the two ordinary-mirrors we change their directions through another beam splitter (or half-silvered mirror) and photon is always detected in the right direction. Our photon is preserving its superposition and interference. However, if we place a block on one path, in Figure 5b, superposition will be broken and destruction of interference occurs.

Now we will look at the similar interference loss which is the source of the decoherence in open quantum systems (computers). Let's think Q as the system of the quantum computer and E as the environment and suppose that Q and E are entangled to each other. The state of the entangled system, EPR state in eq.2.5, is;

$$|\Psi\rangle = \frac{1}{\sqrt{2}}(|0\rangle_Q|0\rangle_E + |1\rangle_Q|1\rangle_E) \qquad (2.6)$$

Use an unitary transformation called Hadamard on the system and a measurement on the final system's state cause loss of interference, like in the previous experiment.

$$\mathrm{H}|0\rangle_{Q,E} = \frac{1}{\sqrt{2}}(|0\rangle_{Q,E} + |1\rangle_{Q,E}) \tag{2.7}$$

$$\mathrm{H}|1\rangle_{Q,E} = \frac{1}{\sqrt{2}}(|0\rangle_{Q,E} - |1\rangle_{Q,E}) \tag{2.8}$$

Then the state is;

$$(½)(|0\rangle_Q|0\rangle_E + |1_Q|0\rangle_E + |0\rangle_Q|0\rangle_E - |1\rangle_Q|1\rangle_E) \tag{2.9}$$

Measurement on Q gives us ½ probability $|0\rangle_Q$ and ½ probability $|1\rangle_Q$, which means interference is destroyed just like in Figure 5b and this situation is a partial description of the classical behavior of A after the measurement.

Let's apply the same transformation on a system which is in a linear combination of $|0\rangle_Q$ and $|1\rangle_Q$;

$$|\Psi\rangle = \frac{1}{\sqrt{2}}(|0\rangle_Q + |1\rangle_Q) \tag{2.10}$$

$$\mathrm{H}|\Psi\rangle = |0\rangle_Q \tag{2.11}$$

Result of a measurement on these systems will be $|0\rangle_Q$ with probability 1, just like in Figure5a.

Quantum computers are quantum mechanical computers and must preserve their quantum nature while quantum operations are used. Therefore, due to this operations there may be correlations between systems leading to disturbance of the the quantum nature (quantum coherence) of the quantum system. There are lots of studies investigating "decoherence time" of various molecular structures [79-81] and this problem can be solved by finding operation speeds faster than decoherence time of these molecular systems.

2.2 Usage of Qubits and Quantum Algorithms

2.2.1 Quantum analogy of classical information units

Classical digital computers use binary system, 0 and 1, to encode information and those bits are manipulated by logic gates based on Boolean algebra. However, a quantum computer's information unit, ***qubit*** can be in a state of a linear combination of $|0\rangle$ and $|1\rangle$; $a|0\rangle + b|1\rangle$, where $|a|^2$ and $|b|^2$ are probabilities of finding $|0\rangle$ and $|1\rangle$, respectively, and $|a|^2 + |b|^2 = 1$ from the normalization condition. Usage of the qubits is not the only possibility to operate a quantum computer but it is the most commonly used one; others are ***qutrits*** and ***qudits***. Firstly a classical ternary (trit) bit system's quantum mechanical analogy is called ***qutrit*** and uses three basis $|0\rangle, |1\rangle$ and $|2\rangle$ or a linear combinations of them;

$$a|0\rangle + b|1\rangle + c|2\rangle \tag{2.12}$$

Secondly, qudits use n-bases (n-level quantum system) or a linear combination of these;

$$a|0\rangle + b|1\rangle + c|2\rangle + \cdots + x|n\rangle \tag{2.13}$$

Power of quantum computers comes from the quantum parallelism in qubit structures. N-qubit system contains 2^n possible states, for example, two qubit quantum system's state is, also called quantum register, written as;

$$|\Psi\rangle = a|00\rangle + b|01\rangle + c|10\rangle + d|11\rangle \tag{2.14}$$

System's state $|\Psi\rangle$ contains two qubits and four components ($2^n=2^2=4$) with $|a|^2 + |b|^2 + |c|^2 + |d|^2 = 1$. When we decide to compute a function, f, we apply an appropriate unitary operation on the system;

$$|\Psi\rangle \rightarrow U|\Psi\rangle=|f(\Psi)\rangle \tag{2.15}$$

$$a|00\rangle + b|01\rangle + c|10\rangle + d|11\rangle \rightarrow a|f(00)\rangle + b\,|f(01)\rangle + c|f(10)\rangle + d|f(11)\rangle \tag{2.16}$$

As a note, only allowed transformations are unitary transformations in quantum computers. Because the Hamiltonian which generates evolution of Schrodinger's equation has its solution only if the linear operator is unitary and quantum superpositions can only be protected by unitary operations. To be more understandable, unitary operations are reversible by inverse operation;

$$U|\Psi\rangle = |\Psi^{\iota}\rangle \tag{2.17}$$

$$U^{-1}|\Psi^{\iota}\rangle = |\Psi\rangle \tag{2.18}$$

The reversibility written in equations 2.17-18 cause preservation of the superposition and conservation of the total probability.

Operation in eq.2.15-16 computes $\boldsymbol{f}$ simultaneously on all four, $2^n=2^2=4$, parts due to quantum parallelism while a classical n-bit sequence or register can index 2^n state but only one state can be stored in the register at a time. However, we have to make a measurement to take this information out of the quantum system and this measurement will destroy the superposition and causes the system to lose its quantum nature, or causes so-called wave function collapse. At this point, we have to design the unitary operations carefully in order that we can obtain the desired solution with highest probability after the measurement. To do this, we need another tool called ***quantum interference***. Quantum interference is used in such a way that the final unobserved quantum system's superposition state contains only the wanted parts those are more likely to be observed after the measurement and so these operations increase the possibility to obtain correct answer. This is like ***constructive*** and ***destructive*** interferences of light. All we have to do is to arrange the correct cancelations by applying suitable unitary transformations or quantum gates to manipulate superposition state. These kinds of operations are the task of special quantum algorithms. We have to keep in mind that quantum computing is a probabilistic computational model and reading the final state of the quantum system must be the final step because measurement operations are destructive. Next section will be more illustrative about this situation.

2.2.2 Deutsch algorithm

Quantum algorithms have great influence on the performance of the quantum computers, as we discuss in the previous section. One of the earliest examples of a quantum algorithm is proposed by D. Deutsch [32] to solve the problem called "Deutsch Problem" and quantum computers are superior to the classical ones for this problem.

Deutsch problem is based on the investigation of whether a function **f: {0,1}→{0,1}** is *constant* or *balance* using only a single input. It is said to be *constant* if f(0)=f(1) and balanced if f(0)≠f(1). Structure of the solution of this problem is based on the ***Deutsch algorithm***. It is important that the problem here is not to find out what f is, but to determine a property of it.

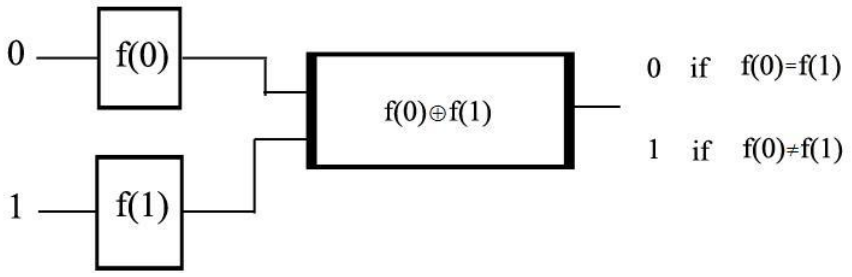

Figure 6: Classical circuit for the solution of Deutsch problem.

Classical computers solve the problem by evaluating f twice; circuit diagram shown in Figure 6 evaluates f(0) and then f(1) and resulting values determine whether f is balanced or constant.

Quantum computational circuit evaluates the problem as follows; firstly Figure 7a shows the evaluation principle, input (first qubit) **x** becomes unchanged after appropriate

unitary operation, U_f, D. Deutsch called it "Oracle" or "Black box" and second qubit **y** becomes y+f(x) (mod 2).

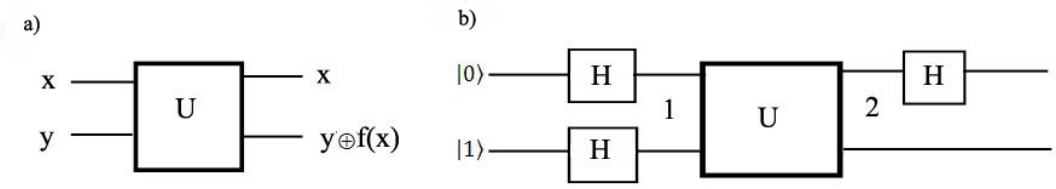

Figure 7**:** Quantum circuit for the solution Deutsch problem a) general computing

structure of a quantum circuit with only one input, x. b) Quantum circuit for the Deutsch algorithm.

Firstly Hadamard transformations (or gates) are acted on $|0\rangle$ and $|1\rangle$, here the usage of the Hadamard gates can be taught as the usage of interference explained in previous the chapter and shown in Figure 5. How Hadamard gates act on qubits shown in Figure 7b is as follows;

$$H|0\rangle = 1/\sqrt{2}(|0\rangle + |1\rangle) \tag{2.19}$$

$$H|1\rangle = 1/\sqrt{2}(|0\rangle - |1\rangle) \tag{2.20}$$

Combined system's state after Hadamard transformations applied is, after the stage **1** shown in Figure 7b;

$$|\Psi\rangle_{combined} = \frac{1}{2}(|0\rangle + |1\rangle)(|0\rangle - |1\rangle) = \frac{1}{2}(|00\rangle - |01\rangle + |10\rangle - |11\rangle) \tag{2.21}$$

We define that $U|x\rangle|y\rangle \rightarrow |x\rangle|y \oplus f(x)\rangle$, by putting $\oplus$ we apply mod 2 to the y+f(x) and after these state enters the oracle (U), system's state according to our definition $U|x\rangle|y\rangle$ is;

$$U\,|x\rangle\otimes|y\rangle=(-1)^{f(x)}|x\rangle\otimes|y\rangle \tag{2.22}$$

$$U\,\frac{(|0\rangle+|1\rangle)}{\sqrt{2}}\otimes\frac{(|0\rangle-|1\rangle)}{\sqrt{2}}=\frac{(-1)^{f(0)}|0\rangle+(-1)^{f(1)}|1\rangle}{\sqrt{2}}\otimes\frac{(|0\rangle-|1\rangle)}{\sqrt{2}} \tag{2.23}$$

We have one more step, stage **2,** to complete the algorithm which is to apply one more Hadamard gate to the first qubit $|x\rangle$ in eq.2.23 after the U operation;

$$|x\rangle=\frac{(-1)^{f(0)}|0\rangle+(-1)^{f(1)}|1\rangle}{\sqrt{2}} \tag{2.24}$$

$$H|x\rangle=(-1)^{f(0)}\left(\frac{|0\rangle+|1\rangle}{\sqrt{2}}\right)+(-1)^{f(1)}\left(\frac{|0\rangle-|1\rangle}{\sqrt{2}}\right) \tag{2.25}$$

Assume possibility of two scenario f(0)=f(1)=0 and f(0)=f(1)=1 i.e. f is constant, then the resulting state, in eq. 2.25, becomes;

$$|x\rangle=\pm\left(\frac{|0\rangle+|1\rangle}{\sqrt{2}}\right)\pm\left(\frac{|0\rangle-|1\rangle}{\sqrt{2}}\right)=\pm|0\rangle \tag{2.26}$$

Then, if f is balanced f(0)≠f(1) with f(0)=0, f(1)=1 and f(0)=1, f(1)=0, resulting state will be;

$$|x\rangle=\pm\left(\frac{|0\rangle+|1\rangle}{\sqrt{2}}\right)\mp\left(\frac{|0\rangle-|1\rangle}{\sqrt{2}}\right)=\pm|1\rangle \tag{2.27}$$

Equations 2.26 and 2.27 assure that if ***f*** is constant our measurement on both final possible states of x shown in eq. 2.25 will give us with certainty the outcome $|0\rangle$ and if ***f*** is balanced, our measurement on both final possible states of x shown in eq. 2.26 will give us with certainty the outcome $|1\rangle$. By applying this algorithm, we gain advantage over the classical computers because using the interference and quantum parallelism we were able to solve the problem with only one operation, or evaluation of ***f***.

It can be also explain with to the Mach-Zehnder interferometer shown in Figure 5 that we can solve the problem with only one photon. Half-silvered mirrors serve as Hadamard transformations in Deutsch algorithm and at this time the problem will be about phase shifters, φ^1, $\varphi^2 \in\{0,\pi\}$ are equal or not ($\varphi^1=\varphi^2$ or $\varphi^1\neq\varphi^2$). All we have to do to find the phase difference φ^1- φ^2 and so determine whether $\varphi^1=\varphi^2$ or $\varphi^1\neq\varphi^2$ by

detecting the direction of photon just like the determination of ***f*** to be constant or balanced. When phases are $\varphi^1=0$, $\varphi^2=\pi$ and $\varphi^1=\pi$, $\varphi^2=0$, outcome will be$|1\rangle$ and $\varphi^1=0$, $\varphi^2=0$ and $\varphi^1=\pi$, $\varphi^2=\pi$, outcome will be $|0\rangle$.

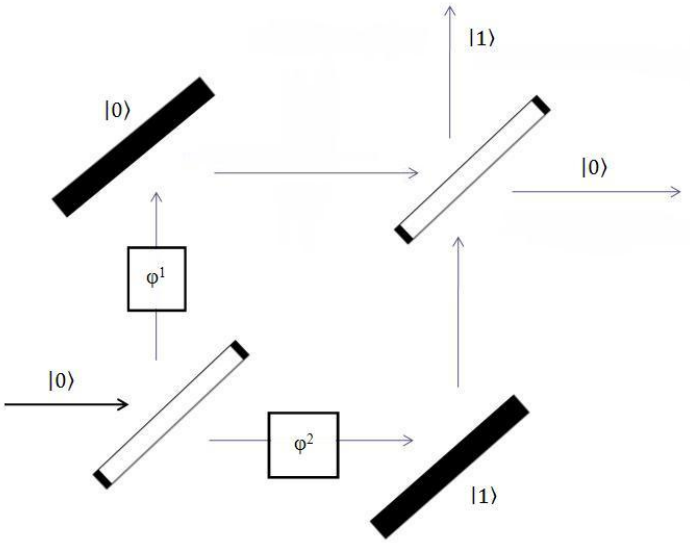

Figure 8: Analogy of the solution of Deutsch problem using Mach-Zehnder interferometer, φ^1 and φ^2 are phase shifters.

2.3 Sympathy for a spin-qubit

Theoretically investigated properties of quantum computers are given in previous chapters taking into account the special structure and phenomenons of quantum physics including interference, superposition, measurement, entanglement and decoherence. However, to construct a working physical implementation of a quantum computer is a very challenging task and the requirements that any physical quantum computer must satisfy are known as ***DiVincenzo criteria*** [82] given by D. DiVincenzo in 2000. Most

important ones are that qubits must be well isolated from the environment to reduce quantum decoherence caused by interaction between system and environment, however, we also need gate operations act much faster than decoherence times of the qubits. Because of the consequences of the no-cloning theorem [83,84] which states that arbitrary quantum states can not be copied, qubits must be initialized to some state such as $|0\rangle$ state before the computation. We should be able to read, or measure, the final state to extract the result. In addition, there must be a possibility of making specific qubit measurements.

There are many physical implementations partly satisfying these requirements including spin-based quantum computation (Nuclear magnetic resonance, Kane, and Loss-Divincenzo quantum computers) [85-87], trapped ions [88-91], optical lattice [92], cavity QED [93-95], superconducting [96-98], topological quantum computers [99,100] and adiabatic quantum computers [101]. Appendix A contains full list of DiVincenzo criteria and the quantum computer proposals based on the U.S Advanced Research and Development Activity (ARDA) report [102].

Recently, there are studies investigating the possibility of usage of fullerene nanostructure based quantum computation [103-107] and two of the promising ones are nanopeapods [108,109] and endohedral fullerenes [110-114] and nuclear and electron spins are the qubit candidades of these proposals. Necessary requirements for these structures is given in Ref [115]. These requirements can be also drived from some of the DiVincenzo's criteria and include charge arrangements of the fullerene, spin density distributions and qubit-qubit interactions.

Electron, nuclear spin and electron orbital state qubits are mainly used in fullerene based proposals of quantum computers and electron spins inside the fullerene based materials have advantages over nuclear spin qubits and great potential to become a qubit candidate. As we have stated that qubit operations are badly affected by the decoherence phenomenon and also operations must act faster than the decoherence times. Figure 9 shows the comparion of decoherence times, or dephasing times, and time scales required for the control of the qubits for electron and nuclear spin qubits. As we

can see from the figure today's fast microprocessors operation time is between the time scales of decoherence and control times, while nuclear and orbitals states time scales can not reach the microprocessors time scales. This makes spin-qubits more favorable over the other qubit proposals.

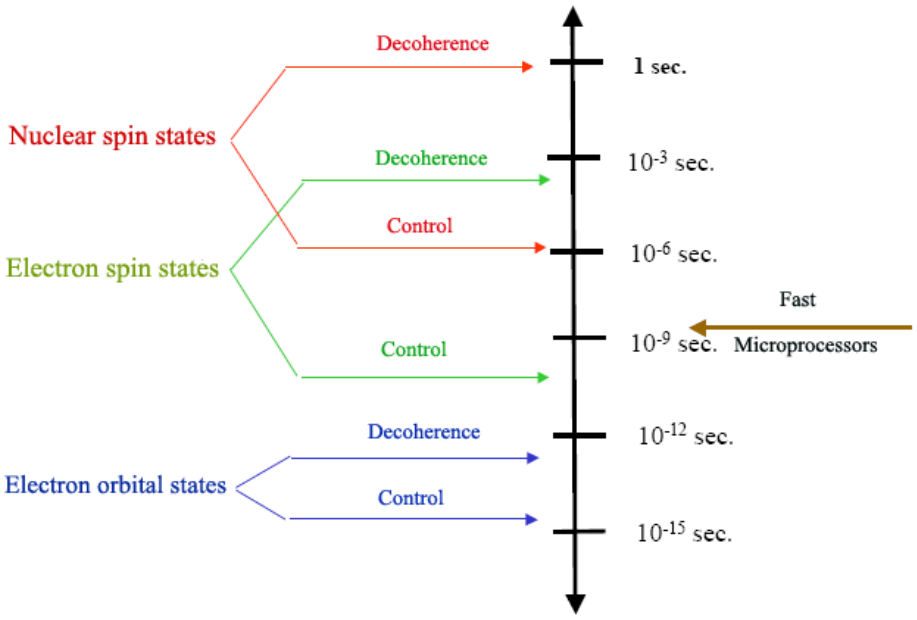

Figure 9: Control and decoherence times of nuclear, electron spin and electron orbital states.

CHAPTER 3

METHODS IN COMPUTATIONAL QUANTUM CHEMISTRY

The purpose of this chapter is to give brief information about theoretical methods used for determining special properties of materials. Theoretical background contained in this chapter is summarized from Refs [116-120].

3.1 Many Body Problem and Adiabatic Approximation

Investigating special properties of molecules using computational chemistry methods on computers rather than experiments is growing field of study in many disiplines such as in physics, chemistry and biology. This kind of investigations including energy, charge distribution, reactivity and geometry optimisation enable us not only to look at the chemical and physical properties but also find the desired modifications on the materials that provide pre-determination of these properties. Moreover, dealing with nanoscale materials is experimentally difficult and so computational studies becomes an important characterization tool in these scales.

Computational quantum chemical methods use tools of quantum mechanics to estimate the properties of materials and some of these are ab-initio methods such as Hartree Fock method, Møller–Plesset perturbation theory [121], configuration interaction (CI) [122,123], multi-configurational self-consistent field (MCSCF) and Density functional theory [124,125]. The need for these methods is caused by the inseparability of many

body schrödinger equation. To understand this, let's write the time-independent schödinger equation :

$$H\Psi = E\Psi$$

$$H = T + V \tag{3.1}$$

$$H = T_n + T_e + V_{nn} + V_{ne} + V_{ee}$$

Where H is the system's many body hamiltonian, T is kinetic energy and V is the potential energy term. Properties of materials is investigated through solving this equation. As shown in eq. system's many body hamiltonian consists of kinetic and potential parts, potential part contains three terms caused by nucleus-nucleus, nucleus-electron and electron electron interactions, V_{nn}, V_{ne}, V_{ee}, respectively and kinetic part consists of two terms which are kinetic energy of nuclei and electron, T_n and T_e, respectively.

$$H = -\sum_{n=1}^{M} \frac{\hbar^2}{2M_n} \nabla^2{}_n - \sum_{e=1}^{N} \frac{\hbar^2}{2m_e} \nabla^2{}_e + \frac{1}{2} \sum_{n \neq k=1}^{M} \frac{1}{4\pi\varepsilon_0} \frac{Z_n Z_k e^2}{|R_n - R_k|} + \frac{1}{2} \sum_{e \neq f=1}^{N} \frac{1}{4\pi\varepsilon_0} \frac{e^2}{|r_e - r_f|} - \sum_{n}^{M} . \sum_{e}^{N} \frac{1}{4\pi\varepsilon_0} \frac{Z_n e^2}{|R_n - r_e|} \tag{3.2}$$

Schrödinger's equation that we have to solve now becomes;

$$H\Psi(\vec{R}, \vec{r}) = (T_n + T_e + V_{nn} + V_{ne} + V_{ee})\, \Psi(\vec{R}, \vec{r}) = E\Psi(\vec{R}, \vec{r}) \tag{3.3}$$

Where R and r are nuclear and electronic coordinates. In order to give an acceptable solution to this inseparable equation, different approximations are applied. Considering electrons' movement much faster than the nuclei (i.e the nuclei can be regarded as fixed) is the basis of Born-Oppenheimer or adiabatic approximation [126]. This appoximation is based on the idea that motions of electron and nuclei can be separated, then the wave function can be written in product form as;

$$\Psi(\vec{R}, \vec{r}) = \Psi(\vec{R}, \vec{r})\Psi(\vec{R}) \tag{3.4}$$

Fixed nuclei causes nuclear kinetic term to become zero, T_n=0, and V_{nn} term to become constant, so the final form of the Eq.3.3 is;

$$H_{\mathrm{e}} = T_{\mathrm{e}} + V_{\mathrm{ee}} + V_{\mathrm{ne}} \tag{3.5}$$

We have now two different Schrödinger equations as we consider Eq. 3.4 and these are shown in Eqs.3.6 and 3.7.

$$(T_e + V_{ee} + V_{\mathrm{ne}})\Psi(\vec{R},\vec{r}) = E_e(R)\Psi(\vec{R},\vec{r}) \tag{3.6}$$

$$(T_n + V_{nn} + E_e(R))\Psi(\vec{R}) = E\,\Psi(\vec{R}) \tag{3.7}$$

Eq.3.6 is called electronic schrödinger equation and $E_e(R)$ are electronic energies. The total energy can be written as;

$$E = E_e(R) + \frac{1}{2}\sum_{n\neq k=1}^{M} \frac{1}{4\pi\varepsilon_0}\frac{Z_n Z_k e^2}{|R_n - R_k|} \tag{3.8}$$

3.2 Hartree-Fock Approximation

Hartree-Fock approximation uses the idea that each electron moves in the average potential field of the other electrons i.e system can be treated as many body system of independent particles. In this method, Schrodinger equation of many-electron system solved with the help of variational principle and many body wave function is created by Slater determinant [127] satisfiying Pauli's exclusion principle and the antisymmetry condition. Therefore, many-body wave function in terms of spin orbitals can be written as;

$$\Psi = \frac{1}{\sqrt{N!}}\begin{vmatrix} \Theta_1(\vec{x}_1) & \Theta_2(\vec{x}_2)\ldots\ldots & \Theta_N(\vec{x}_1) \\ & \vdots & \vdots \\ \Theta_N(\vec{x}_1) & \Theta_2(\vec{x}_2)\ldots\ldots & \Theta_N(\vec{x}_N) \end{vmatrix} \tag{3.9}$$

Hamitonian of an atom with N electrons can be written as;

$$H = \sum_{i=1}^{N} h_1(x_i) + \sum_{i<j}^{N} h_2(x_{i,j}) \tag{3.10}$$

Where $h_1(x_i)$ is single particle hamiltonian of i$^{\mathrm{th}}$ particle and $h_2(x_{i,j})$ is the interaction between i and j particles. $h_1(x_i)$ and $h_2(x_{i,j})$ is written as (in a.u.);

$$h_1(x_i) = -\frac{1}{2}\nabla_{\mathrm{i}}{}^2 - \frac{Z}{r_i} \tag{3.11}$$

$$h_2(x_{i,j}) = \frac{Z}{|r_i - r_j|} \tag{3.12}$$

Choosing $\Theta_N(\vec{x}_1)$, $\Theta_2(\vec{x}_2) \ldots \Theta_1(\vec{x}_N)$ as orthonormal, expectation value of the Hamiltonian in Eq.3.10 (or total energy of the Hartree-Fock method) is found by inserting Ψ in slater deteminant form into the Eq.3.10.

$$\langle \Psi|H|\Psi\rangle = \sum_{i=1}^{N}\langle \Theta_i|h_1|\Theta_i\rangle + \frac{1}{2}\sum_{i,j}^{N}\{\langle \Theta_i\Theta_j|h_2|\Theta_i\Theta_j\rangle - \langle \Theta_j\Theta_i|h_2|\Theta_i\Theta_j\rangle\} \tag{3.13}$$

$$\mathrm{E_{HF}} = \sum_{i=1}^{N} A_i + \frac{1}{2}\sum_{i,j}^{N}\{\mathrm{B_{ij}} - \mathrm{C_{ij}}\} \tag{3.14}$$

Here, $\mathrm{B_{ij}}$ is called Coloumb and $\mathrm{C_{ij}}$ is called Exchance integral terms. By applying Lagrange multipliers method we protect the normalization constraint $\langle \Theta_i|\Theta_j\rangle = \delta_{ij}$ (minimization of expectation value) and the equation of constraint is multiplied by some constant and it is added to the equation which is to be minimized. Our constrait equation is $\langle \Theta_i|\Theta_j\rangle - \delta_{ij} = 0$. The new expectation value of the hamiltonian is;

$$F = \langle \Psi|H|\Psi\rangle - \sum_{i,j}^{N} Z_{ij}\ (\langle \Theta_i|\Theta_j\rangle - \delta_{ij}) \tag{3.15}$$

$$\delta F = \delta E - \sum_{i,j}^{N} Z_{ij}\ \delta(\langle \Theta_i|\Theta_j\rangle) = 0 \tag{3.16}$$

What we do here is to use functional derivatives and insert new orbitals $|\Theta_i\rangle \rightarrow |\Theta_i\rangle + |\delta\Theta_i\rangle$ into Eq.3.15. After some long calculations which is not included here but readers looking for more detailed calculations can see Ref [116], we find the Hartree-Fock equation and Hartree-Fock operator, F as follows;

$$[h_1 + \sum_{i=1}^{N}(B_i - C_i)]\Theta_k = \sum_{i=1}^{N} Z_{ki}\ \Theta_i \tag{3.17}$$

$$F\ \Theta_k = \sum_{i=1}^{N} Z_{ki}\ \Theta_i \tag{3.18}$$

We have to keep in mind that Hartree-Fock method is a wave function based method and atomic orbitals (AOs) represented by functions that can be Hydrogen like, Slater and Gaussian functions. We define basis functions ω_i, which are used to write molecular orbitals as linear combinations of atomic orbitals (LCAO approximation), $\Theta_k = \sum_{i=1}^{N} A_{ik}\ \omega_i(x)$, in order to overcome the difficulty of solving the HF equations. Because still evaluation of these equations is a hard task. Idea of basis function expansion is proposed by Roothaan.

Slater type orbitals (STO)[127] and Gaussian-type orbitals (GTO) are given in Eqs.3.19 and 3.20. STOs are not orthogonal while GTOs are orthogonal orbitals.

$$\omega(r) = \frac{(2\mu)^{n+\frac{1}{2}}}{(2n!)^{\frac{1}{2}}} r^{n-1} e^{-\mu r}\, Y_{lm}(\theta, \emptyset) \tag{3.19}$$

$$\omega(r) = \frac{(2)^{n+1}\alpha^{(2n+1)/4}}{[(2n+1)!]^{\frac{1}{2}}(2\pi)^{1/4}} r^{n-1} e^{-\alpha r^2}\, Y_{lm}(\theta, \emptyset) \tag{3.20}$$

Basis sets STO-nG [128] in which n represents the number of Gaussians to approximate Slater Type Orbitals (it means expantion of each Slater Type Orbital (STO) in three GTO) are known as minimal basis sets expansion or smallest basis sets. They are preferentially to used in large molecules.

Extended basis sets by definition gives more detail about orbitals. Double-Zeta, Triple-Zeta, Quadruple-Zeta, Diffuse Sets, Split-Valence and Polarized Sets are examples of such basis sets. Approximation of orbitals gives the same orbital shape in minimal basis sets but Double-Zeta functions are obtained by expressing each atomic orbital as the sum of two STOs. Eq.3.21 is the example for the 2s orbitals;

$$\omega(r) = \omega^{STO}(r, \zeta_1) + A\omega^{STO}(r, \zeta_2) \tag{3.21}$$

Different ζ means different orbital sizes and constant A represents the second's orbitals contribution. Triple-Zeta and Quadruple-Zeta consist of three and four STOs, respectively.

Split-Valence basis sets are described by the representation of inner-shell electrons with single STO. They are suitable for the calculations in which the contribution of the core electrons contribution is very small. Some examples of SV basis sets are 3-21G [129] and 6-31G [130]. In this representation, 3 (in 3-21G) and 6 (in 6-31G) means number of Gaussian functions (GTO) used to construct inner-shell orbital. Numbers 2 (in 3-**2**1G) and 3 (in 6-**3**1G) are the number of gaussian functions that form first Slater type orbital

of the double zeta and finally 1 (in 3-2**1**G and 6-3**1**G) mean number of GTOs in the second double zeta.

3.3 Density Functional Theory

The idea behind the Density Functional Theory (DFT) is to represent the fermionic systems as electron density instead of many body wave functions. The main advantage of this idea is that wave functions have complete information of the system but a system with N electrons depends on 3N spatial and N spin coordinates and this dependence on too many variables. In addition, interactions in a realistic system, like V_{ee}, are very time consuming processes. Although the idea of representing total energy as electronic density is proposed by Thomas and Fermi [131-133], structure of the of DFT is constructed by two theorems of Hohenberg-Kohn [134] and equations of Kohn–Sham [135].

3.3.1 Hohenberg-Kohn Theorems

Hohenberg-Kohn's first theorem states that V_{ne} potential term in the system's hamiltonian is uniquely determined by electron density (ρ) which means that same ground state electronic density is not achieved by two different potential i.e. each V_{ne} corresponds only one ground state density (there is a one to one correspondence between them). The total energy can be written in functional form as follows;

$$E[\rho] = T[\rho] + V_{ne}[\rho] + V_{ee}[\rho] \tag{3.22}$$

$$V_{ne}[\rho] = \int \rho(\vec{r}) v(\vec{r}) dr \tag{3.23}$$

Term $T[\rho]+V_{ee}[\rho] = F_{HK}$ is known as Hohenberg-Kohn functional and it does not depend on $v(\vec{r})$ potential. It can be seen from the first theorem that knowing $\rho(r)$ gives $v(\vec{r})$ and so Ψ, therefore gives all the electronic properties.

Hohenberg-Kohn's second theorem uses the energy variational principle and states that the density that minimizes the total energy is the exact ground state density. Any arbitrary electron density $\rho(r)$ satisfy the conditions;

$$\rho(r) \geq 0 \quad \text{and} \quad \int \rho(r)dr = N \tag{3.24}$$

Lowest energy E_0 is only given as a functional of real ground state density ρ_0 and $E_0 = E[\rho_0] \leq E[\rho]$ which is analogous for variational principle of wavefunction $E_0 \leq E[\Psi]$.

Energy minimization applied with the constraint given in Eq.3.24 with the Lagrange multipliers method to maintain this constraint just like we did in Hartree-Fock method is as follows;

$$\delta\{E[\rho] - \mu[\int \rho(r)dr - N]\} = 0 \tag{3.25}$$

It gives Euler-Langrange equation;

$$\mu = \frac{\delta E[\rho]}{\delta \rho(\vec{r})} = v(\vec{r}) + \frac{\delta F_{HK}[\rho]}{\delta \rho(\vec{r})} \tag{3.26}$$

If we know the functional $F_{HK}[\rho]$, problem of ground state determination will change to the issue of minimization of a functional of electron density. Note that energy functional F_{HK} is unknown and we have to deal with approximate energy functionals.

3.3.2 Kohn-Sham Method

The Kohn-Sham method based on approximating the kinetic energy term given in Eq.3.22 and also inside the Hohenberg-Kohn functional F_{HK}. The method considers a system of N non-interacting particles in some external potential v_{KS} to find the kinetic energy of the interacting system.

Method gives the wave function of the non-interacting system Ψ composed of N orbitals which are lowest eigenstates of non-interacting hamiltonian, kinetic energy $T_{non}[\rho]$, total hamiltonian H_{non} and ground state density $\rho(r)$ in an external potential as;

$$\Psi = \frac{1}{\sqrt{N!}} |\emptyset_1 \emptyset_2 \dots \emptyset_N| \tag{3.27}$$

$$T_{non}[\rho] = \sum_{i=1}^{N} \left\langle \emptyset_i \left| -\frac{1}{2}\nabla^2 \right| \emptyset_i \right\rangle \tag{3.28}$$

$$H_{non} = -\frac{1}{2}\nabla^2 + v_{KS}(r) \tag{3.29}$$

$$\rho(\vec{r}) = \sum_{i=1}^{N} |\emptyset_i(r)|^2 \tag{3.30}$$

As a note Hohenberg-Kohn's first theorem is valid for this non-interacting system.

Then, the system's total energy $E[\rho]$ can be written as;

$$E[\rho] = T_{non}[\rho] + \int v(r)dr + J[\rho] + E_{xc}[\rho] \tag{3.31}$$

$$J[\rho] = \frac{1}{2}\iint \frac{1}{r_{12}} \rho(r_1)\, \rho(r_2) \mathrm{d}r_1 \mathrm{d}r_2 \tag{3.31}$$

$$E_{xc}[\rho] = (T[\rho] - T_{non}[\rho]) + (V_{ee}[\rho] - J[\rho]) \tag{3.32}$$

Where $J[\rho]$ is the classical repulsion i.e. electrostatic energy of the charge density and $E_{xc}[\rho]$ is the exchange-correlation energy and has constributions of many body correlation and exchange.

All we have to do now is to minimize $E[\rho]$ using variational principle;

$$\delta E[\rho] = \delta T_{non}[\rho] + \delta\left[\int v(r)dr + J[\rho] + E_{xc}[\rho]\right] = 0 \tag{3.33}$$

We can find the $\delta T_{non}[\rho]$ term by giving non-interacting energy functional;

$$E_{non}[\rho] = \sum_{i=1}^{N} \left\langle \emptyset_i \left| -\frac{1}{2}\nabla^2 + v_{KS} \right| \emptyset_i \right\rangle \tag{3.34}$$

$$= T_{non}[\rho] + \int v_{KS}\rho(r)dr \tag{3.35}$$

And a variation of $\delta\rho(r)$ gives;

$$\delta E_{non}[\rho] = \delta T_{non}[\rho] + \int v_{KS}\delta\rho(r)dr = 0 \tag{3.36}$$

$$\delta T_{non}[\rho] = -\int v_{KS}\delta\rho(r)dr \tag{3.37}$$

Final form is;

$$\delta E[\rho] = \delta T_{non}[\rho] + \int dr \left[v(r) + \frac{\partial J[\rho]}{\partial \rho(r)} + \frac{\partial E_{xc}[\rho]}{\partial \rho(r)} \right] \delta\rho(r) = 0 \tag{3.38}$$

$$\delta E[\rho] = -\int v_{KS} \delta\rho(r) dr + \int dr \left[v(r) + \frac{\partial J[\rho]}{\partial \rho(r)} + \frac{\partial E_{xc}[\rho]}{\partial \rho(r)} \right] \delta\rho(r) = 0 \tag{3.39}$$

We obtain potentials v_J and v_{xc} from Eq.3.34;

$$v_J = \frac{\delta J[\rho]}{\delta \rho(r)} = \int \frac{\rho(r')}{|r - r'|} \tag{3.40}$$

$$v_{xc} = \frac{\delta E_{xc}[\rho]}{\delta \rho(r)} \tag{3.41}$$

Then, the Kohn-Sham potential can be taken from $\delta E[\rho]$ and written as $v_{KS} = v(r) + v_J + v_{xc}$ and total energy can be computed directly from Eq.3.33.

The problem arises because of the exchange-correlation functional because we don't know its correct form and there are possible functionals including local density approximation (LDA) and generalized gradient approximation (GGA) and other hybrid methods.

Local density approxiamation (LDA) is defined as;

$$E_{xc}^{LDA}[\rho] = \int \rho(r) \epsilon_{xc}(\rho)\, dr \tag{3.42}$$

Where ϵ_{xc} is defined as exchange-correlation per electron and corresponding potential v_{xc}^{LDA} is;

$$v_{xc}^{LDA} = \frac{\delta E_{xc}^{LDA}[\rho]}{\delta \rho(r)} = \epsilon_{xc}(\rho) + \rho(r) \frac{\delta \epsilon_{xc}(\rho)}{\delta \rho(r)} \tag{3.43}$$

Common LDA functinals are Perdew-Zunger [136], M. Teter-Pade[137] and Vosko-Wilk-Nusair [138].

The Local Spin Density Approximation (LSDA), on the other hand, uses two spin densites ρ_1 and ρ_2 from which we can drive relations for exchange-correlation term for systems with uneven spin density distributions called spin-polarized systems.

Generalized gradient approximation (GGA) is the improved version of LDA to the inhomogenous systems. Here local exchange-correlation energy depends also on the local density gradient. Exchange-correlation energy functinal is written as;

$$E_{xc}^{LDA}[\rho] = \int f(\rho(r), \nabla\rho(r))\, dr \tag{3.44}$$

Examples of GGA are Becke [140], Perdew [141] and Perdew and Wang [142].

There are also hybrid methods that combine Hartree Fock exact exchange and LDA/GGA exchange-correlations. The simplest of these methods is half-and-half functional which is written as;

$$E_{xc}^{H+H} = \frac{1}{2}E_x^{HF} + \frac{1}{2}E_{xc}^{DFT} \tag{3.45}$$

There is an improved version of this called B3LYP[143-145] and it is written as;

$$E_{xc}^{B3LYP} = E_{xc}^{LDA} + a(E_x^{HF} - E_x^{LDA}) + b(E_x^{GGA} - E_x^{LDA}) + c(E_c^{GGA} - E_c^{LDA}) \tag{3.46}$$

Where a,b and c are determimed by fitting expermental data.

CHAPTER 4

UNDERSTANDING SPIN-QUBIT PROPERTIES AND ENDOHEDRAL C_{60} FULLERENES AS A START

4.1 Introduction

Carbon based materials have attracted much interest in chemistry, physics, biology and material science after the discovery of C_{60} fullerenes [14], endohedral fullerenes [146] and carbon nanotubes [13]. In addition, lots of theoretical and experimental studies have been carried out in order to investigate the use of these structures in molecular electronics [147,148], drug delivery systems [149-151] and in the field of superconductivity [152-154] etc. Furthermore, a number of researches on fullerene systems which include $N_4@C_{60}$ [155], $K@C_{60}$ [156,157], $La@C_{82}$ [158-160], $Li@C_{60}$ [161,162], $GeH_4@C_{60}$ [163], $Kr@C_{60}$ [164], $Y@C_{60}$ [165], $Sc_3N@C_{80}$ [166], $La_2@C_{78}$ [167,168], $Sr@C_{60}$ [169], $Be@C_{60}$ [170,171] are reported in various articles studied both as fullerenes and peapod structures and carbon fullerenes are not the only kind that studied experimentally and theoretically.

Endohedrally doped fullerene chains can be a promising candidates in spin based quantum computer proposals because especially carbon based materials are believed to have long spin coherence times due to low spin orbit coupling and provide preserved electronic properties allowing well defined spin-qubits. Nuclear and electron spins of metal and non-metal atoms inside the fullerenes can serve as spin-qubits in these systems. Although there not many studies in this field especially in the field of electronic structure calculations for spin-qubit properties, studies are increasing every year.

Possible qubit candidate studies are $N@C_{60}$ [172-177], $Sc@C_{82}$ [178,179], $P@C_{60}$ [180,181] and $Na@C_{60}$ [182].

Necessary requirements of successful implementation of a quantum computer system known as DiVincenzo's five criteria[82] mentioned in previous chapters including long coherence times, qubit-specific measurement, universal quantum gates, initialization to a pure state and scalable physical system with well-defined qubits. Furthermore, requirements for fullerene based spin-qubits including the studies of charge arrangements, spin distributions and interaction mechanisms are given in Ref [183]. The possibility of a two-qubit operation studies in these systems is based on the investigation of singlet-triplet configurations of the spin-qubits to find the possibility of Heisenberg exchange physical interaction between coupled spins [178] and the necessary value of the exchange coupling for a suitable quantum gate operation is 0.1 meV [184]. The theoretical study on interactions between spin clusters can be found in [185].

In this chapter (and all the other following chapters), we carried out DFT calculations on endohedral fullerenes $Li@C_{60}$, $Na@C_{60}$, $N@C_{60}$ and $P@C_{60}$ with hybrid exchange-correlation density functional of Becke, Lee, Parr and Yang(B3LYP[186-188] using 6-31G basis set [189] in parallel Gaussian03 [190] package. We calculated electron density distributions and electronic configurations and these are found by applying Natural population analysis(NPA) [191] and Mulliken population analysis(MPA) [192]. The optimization of each model considered was carried out as follows; Molecular mechanics [193] method with MM+ force field [194] has been applied first, then Hartree-Fock method [195] with various basis sets (starting from STO-3G up to 6-31G) have been performed. As a final stage DFT/B3LYP/6-31G was applied with the default precision value of the Gaussian-03 software.

4.2 Li and Na Doped C_{60} Fullerenes

In the calculated optimized geometries, Li and Na is located nearly at the center of the C_{60} cages. Minimum and maximum Li-C and Na-C distances are 3.522/3.611 Å for

Li@C_{60} and 3.46/3.687 Å for Na@C_{60}. Optimized geometries with the charge arrangements of the Li and Na doped C_{60} is given in Figure 10.

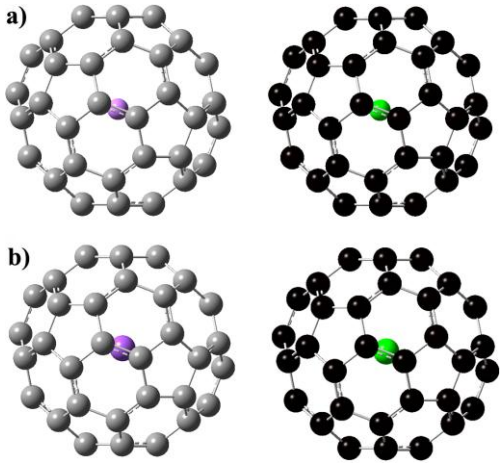

Figure 10: Optimized geometries and MPA/NPA charge arrangements of a) Doublet Li@C_{60} and b) Doublet Na@C_{60}.

As shown in Table 3, singlet-triplet and doublet-quartet energies of empty C_{60} and Li@C_{60} and Na@C_{60} endohedral fullerenes show that singlet state of empty C_{60} and doublet states of Li@C_{60} and Na@C_{60} are energetically more favorable and encapsulation of Li and Na reduces the HOMO-LUMO gap. Energy difference between HOMO-1 and HOMO is 1.914 eV and HOMO-LUMO gap is 0.820 eV for Li@C_{60}. The same quantities are, respectively, 1.926/0.822 for Na@C_{60}. These calculated values are suitable for spin qubit applications.

Table 3: Total energies, E_T, and HOMO-LUMO energy gaps, E_g, of empty C_{60}, Li@C_{60}, Na@C_{60} for differentspin multiplicites (M).

System	M	E_T(a.u.)	E_g(eV)
C_{60}	1	-2285.58896	2.8741
	3	-2285.52325	1.0721
Li@C_{60}	2	-2293.0929	0.8199
	4	-2293.0266	0.8321
Na@C_{60}	2	-2447.8865	0.8223
	4	-2447.8201	0.8308

Charge transfer is from Li and Na to the C_{60} cage and charges on Li and Na are +1.047/+0.831 and 0.912/0.840 according to Mulliken and NPA methods, respectively. NPA charges for both structures are lower than the Mulliken charges. Charges and electronic configurations are shown in Table 4. NPA electronic configurations for both metal atoms encapsulated inside the cage show that electrons have less tendency to spread the upper orbitals than they have in gross orbital populations.

Table 4: Charges and electronic configurations of Li and Na insidethe C_{60} cage.

	Li	Na
Mulliken Charge	+1.047	+0.912
NPA Charge	0.831	+0.840
Gross orbitals	$3s^{0.08}3p^{0.20}4s^{0.06}4p^{0.11}$	$3s^{0.08}3p^{0.20}4s^{0.06}4p^{0.11}$
NPA	$2s^{0.13}2p^{0.03}3s^{0.01}3p^{0.01}$	$3s^{0.14}3p^{0.02}4s^{0.01}$

Figure 11 shows frontier molecular orbitals (MOs) and spin density distribution of $Li@C_{60}$ and $Na@C_{60}$ endohedral fullerenes. HOMO, LUMO and spin density is distributed around the cage for both cases, furthermore HOMO is identical to spin density distribution for both structures.

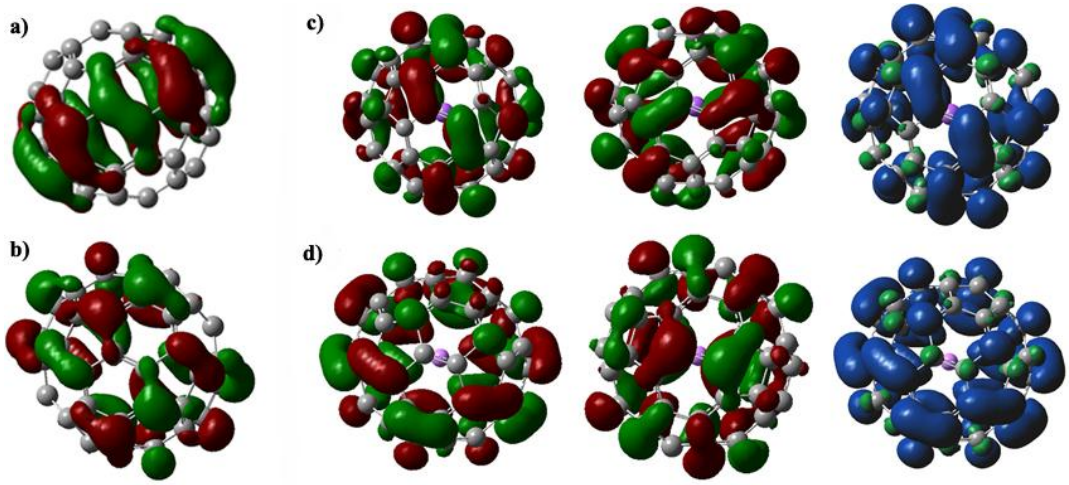

Figure 11: a) HOMO of singlet C_{60} b) LUMO of singlet C_{60} and HOMO, LUMO, Spin density graphics of c) $Li@C_{60}$ d) $Na@C_{60}$, green and red colors represent the positive and negative isosurfaces for HOMO, LUMO, respectively, whereas green and blue colors in spin density graphics represent alpha and beta spins, respectively.

4.3 N and P Doped C_{60} Fullerenes

In the optimized geometry, N and P is located almost at the center of the C_{60} cage. Minimum and maximum N-C distances are 3.514/3.610 Å and P-C distances are

3.545/3.581 Å. Figure 12 shows optimized geometries including the MPA and NPA charge distributions.

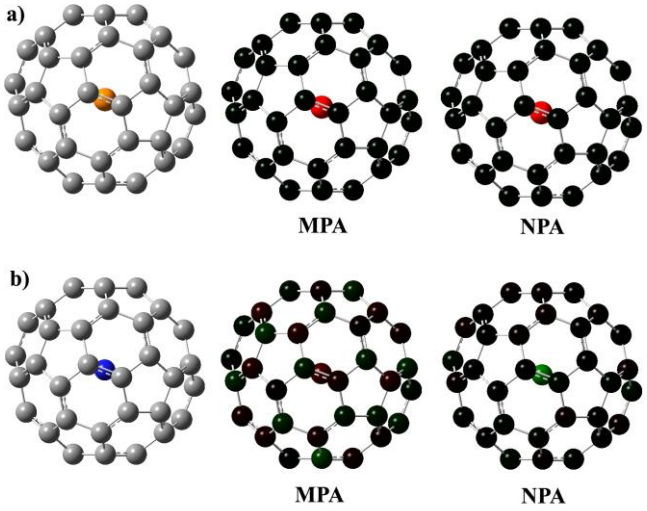

Figure 12: Optimized geometries and MPA-NPA charge arrangements of a) Quartet $P@C_{60}$ and b) Quartet $N@C_{60}$.

Total energies of different spin multiplicites of N and P doped fullerenes are shown in the Table 5, quartet states of both non-metal doped fullerenes are lower in energy and encapsulation of N and P reduces the HOMO-LUMO gap. Energy difference between HOMO-1 and HOMO is 0.00081 eV and HOMO-LUMO gap is 1.498 eV for $N@C_{60}$. On the other hand, $P@C_{60}$ has HOMO-LUMO gap of 2.871 eV and HOMO-(HOMO-1) gap of 0.0011 eV.

Charge transfer is from C_{60} to N in Mulliken analysis and from N to the cage in NPA analysis, charge transfer of $P@C_{60}$ is from the cage to the P in both methods. Excess charge on N is -0.00034/+0.00076 and on P is -0.0293/-0.0294 according to Mulliken and NPA methods, respectively. It is interesting that the elements N and P are not

Table 5: Total energies, E_T, and HOMO-LUMO energy gaps, E_g, of empty C_{60}, N@C_{60} and P@C_{60} for different spin multiplicites (M).

System	M	E_T(a.u.)	E_g(eV)
C_{60}	1	-2285.58896	2.8741
C_{60}	3	-2285.52325	1.0721
N@C_{60}	2	-2340.12564	1.4980
	4	-2340.16988	2.873
P@C_{60}	2	-2626.79381	2.3930
	4	-2626.82056	2.8710

interacting much with the C_{60} cage and retain their atomic configurations, therefore cages can provide protection by isolating the non-metal atoms against the environment and can fulfill one of the DiVincenzo's criteria by giving the possibility of providing long coherence times. Charges and electronic configurations are shown in Table 6. NPA electronic configurations for both metal atoms encapsulated inside the cage show that

Table 6: Charges and electronic configurations of N and P inside the C_{60} cage.

	N	P
Mulliken Charge	-0.00034	-0.0293
NPA Charge	+0.00076	-0.0294
Gross orbitals	$2s^{0.945}2p^{1.926}3s^{1.056}3p^{1.077}$	$3s^{1.355}3p^{1.999}4s^{0.647}4p^{1.067}$
NPA	$2s^{2.00}2p^{3.00}$	$3s^{2.00}3p^{3.02}4p^{0.01}$

electrons have less tendency to spread the upper orbitals than they have in gross orbital populations.

Figure 13 shows frontier MOs and spin density distribution of $N@C_{60}$ and $P@C_{60}$. HOMO-LUMO orbitals are distributed around the cages for both $N@C_{60}$ and $P@C_{60}$ fullerenes, while spin density is mainly concentrated on the N and P (inside the cage). Preserved electronic configurations of these non-metal doped fullerenes can yield long decoherence times which is in a good agreement with[197-199]. Besides, $N@C_{60}$ and $P@C_{60}$ are already two of the strongest spin-qubit candidates[200-205] in solid state quantum computer proposals.

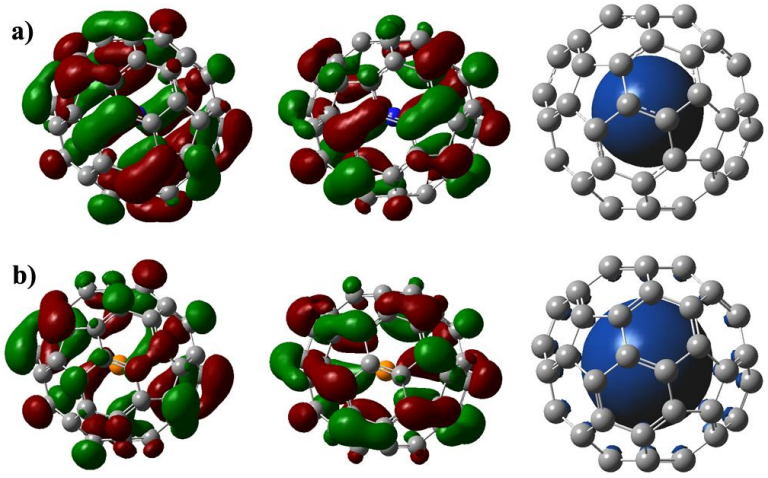

Figure 13: HOMO, LUMO, spin density graphics of a) $N@C_{60}$ and b) $P@C_{60}$, green and red colors represent the positive and negative isosurfaces for HOMO, LUMO, respectively, whereas green and blue colors in spin density graphics represent alpha and beta spins, respectively.

CHAPTER 5

ELECTRONIC AND GEOMETRICAL STRUCTURE OF METAL AND NON-METAL DOPED C_{60} DIMERS

5.1 Li and Na Doped C_{60} Dimers

Geometries of the two metals (Li,Na) doped C_{60} fullerene dimers are based on two C_{60} cages bonded through two carbon atoms with bond distances 1.596/1.596 Å for triplet state of the Li@C_{60} dimer and 1.593/1.591 Å for triplet state of the Na@C_{60} dimer. Figure 14 shows the [2+2] bond distances of the optimized geometries and charge arrangements of the the dimers. Na atoms are not at the center of the fullerenes in the optimized geometry of triplet Na@C_{60} dimer, while Li atoms are located at the center of the structure. Minimum/maximum Li-C distances are 3.452/3.837 Å for the first Li@C_{60} and 3.508/3.949 Å for the second one with Li-Li distances of 9.186 Å. Minimum/maximum Na-C distances are 2.760/4.400 Å and 2.881/4.401 Å with Na-Na distance of 9.675 Å. Double C=C bond formations, shown in Figure 14d, are observed on two hexagons near the linkage of two C_{60} cages of the triplet Li@C_{60} and Na@C_{60} dimers in the optimized geometries.

Energies and HOMO-LUMO energy gaps of the empty C_{60}, Li@C_{60} and Na@C_{60} dimers for different spin multiplicities are given in Table 7. Triplet state of both structures are lower in energy with singlet-triplet energy separation of 0.244 and 0.227 eV.

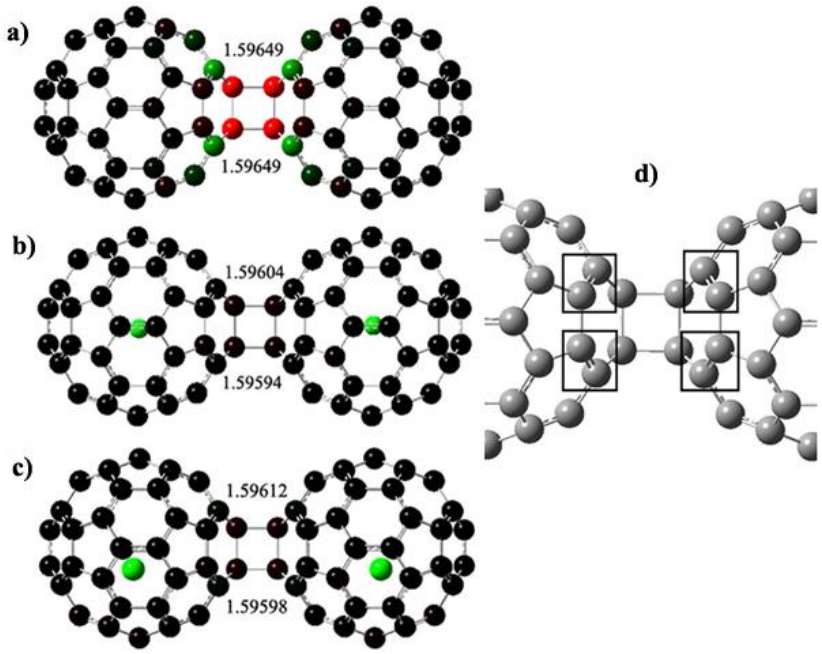

Figure 14: Optimized geometries and charge arrangements of a) C_{60} dimer b) Li@C_{60} dimer c) Na@C_{60} dimer d) Double bond formations near the linkage sides, red and green colors represent negative and positive charges.

Table 7: Total energies, E_T, and HOMO-LUMO energy gaps, Eg, of empty C_{60}, Na@C_{60} and Li@C_{60} dimers for different spin multiplicites.

System	M	E_T(a.u.)	E_g(eV)
C_{60} dimer	1	-4571.1670	2.6158
	3	-4571.1066	1.0052
Li@C_{60} dimer	1	-4586.1689	0.3382
	3	-4586.1779	0.7897
Na@C_{60} dimer	1	-4895.7645	0.5216
	3	-4895.7728	0.7921

Triplet $Li@C_{60}$ dimer has HOMO-LUMO gap of 0.7897 eV and HOMO-(HOMO-1) energy gap of 0.031 eV. Triplet state of $Na@C_{60}$ dimer has HOMO-LUMO gap of 0.7921 eV and HOMO-(HOMO-1) energy gap of 0.0331 eV. Studied Charge transfer mechanisms given in Table 8 using Mulliken and natural population analysis show that electron transfer is from two Li to the C_{60} cages, 1.032-1.032(Mulliken)/0.832-0.832(NPA), and two Na to the C_{60} cages, 0.819-0.820(Mulliken)/0.870-0.870(NPA).

Table 8: Charges and electronic configurations of Li and Na inside triplet $Na@C_{60}$ and triplet $Li@C_{60}$ dimers.

	Li-Li	Na-Na
Mulliken Charge	+1.032,+1.032	+0.819,+0.820
NPA Charge	+0.832,+0.832	+0.870,+0.870
Gross orbitals	$2s^{0.05}2p^{0.22}3s^{0.04}3p^{0.26}$	$3s^{0.09}3p^{0.20}4s^{0.04}4p^{0.05}$
	$2s^{0.05}2p^{0.22}3s^{0.04}3p^{0.26}$	$3s^{0.09}3p^{0.20}4s^{0.04}4p^{0.05}$
NPA	$2s^{0.01}2p^{0.01}3s^{0.12}3p^{0.03}$	$3s^{0.11}3p^{0.01}4s^{0.01}$
	$2s^{0.01}2p^{0.01}3s^{0.12}3p^{0.03}$	$3s^{0.11}3p^{0.01}4s^{0.01}$

HOMO, LUMO and spin density distributions are given in Figure 15. HOMO, LUMO and spin density distributions are around the cages and HOMO and spin densities are almost identical for both dimers. Charges and electronic configurations given in Table 8 show the presence of an interaction between cages and metal atoms. In contrast to natural electron configurations electrons have a tendency to stay at the p orbitals for the metal atoms inside the two dimers.

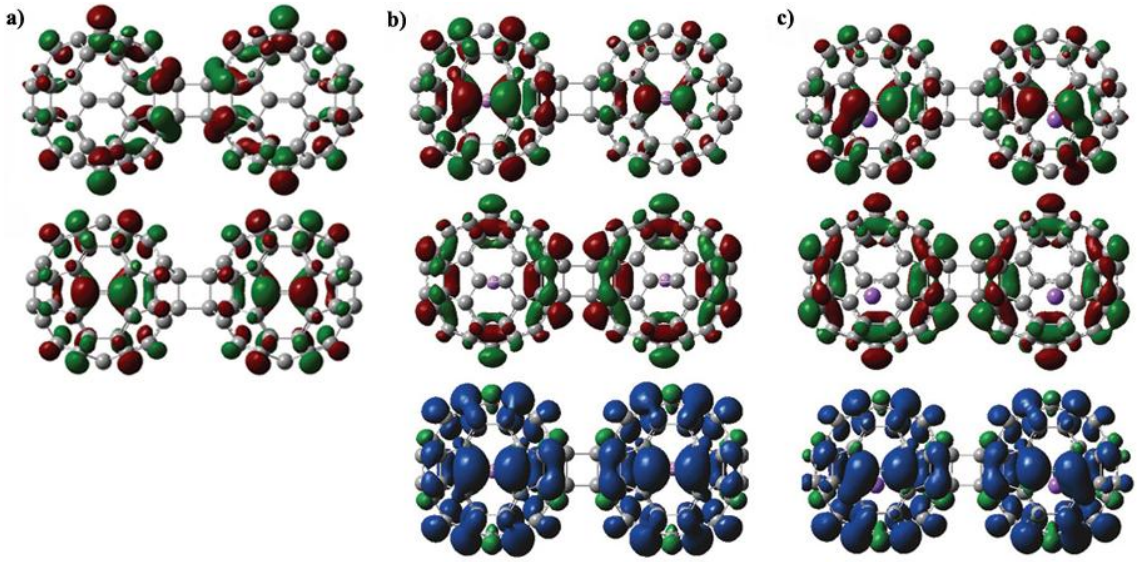

Figure 15: HOMO and LUMO graphics of a) empty C_{60} dimer b) Li@C_{60} dimer c) Na@C_{60} dimer, green and red colors represent the positive and negative isosurfaces for HOMO-LUMO, whereas green and blue colors in spin density graphics represent alpha and beta spins.

5.2 N and P Doped C_{60} Dimers

Two non-metals (N,P) doped C_{60} fullerene dimers are bonded through two carbons with two C-C bond distances of 1.597 Å and 1.597 Å for N@C_{60} dimer and 1.596 Å and 1.596 Å for P@C_{60} dimer. Figure 16 shows the optimized geometries with [2+2] bond distances of both structures. Both atoms N and P are located near the center of the optimized structures. Minimum-maximum N-C distances are 3.508/3.840 Å and 3.480/3.937 Å. Minimum-maximum P-C distances are 3.484/3.818 Å and 3.535/3.863 Å. Compared to the Li-Li and N-N distances of 9.18639 Å and 9.18599 Å, respectively, and min/max distances, P@C_{60}-P@C_{60} dimer has P-P distance of 9.09439 Å which means P

atoms are closer to each other. Double C=C bond formation occurs on two hexagons of each C_{60} cage after full optimization of both dimers.

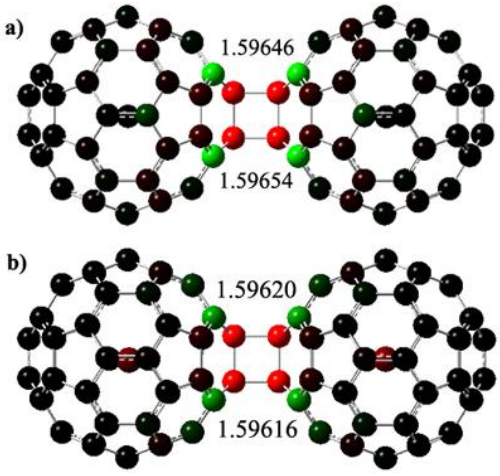

Figure 16: Optimized geometries and charge arrangements of a) N@C_{60} dimer b) P@C_{60} dimer, red and green colors represent negative and positive charges.

Energies and HOMO-LUMO energy gaps of the empty C_{60}, N@C_{60} and P@C_{60} dimers for different spin multiplicities are given in Table 9. Singlet state of N@C_{60} and triplet state of P@C_{60} dimers are lower in energy with singlet-triplet energy separation of 1.203 eV and 0.728 eV, respectively

HOMO-LUMO gap of N@C_{60} dimer is 2.589 eV and HOMO-(HOMO-1) energy gap is 0.056 eV and the same quantities are, respectively, 2.566/0.057 for P@C_{60} dimer. Calculated charge transfer values using Mulliken and natural population analysis indicate that electron transfer is from C_{60} cages to the N with excess charges -0.0014/-0.0016 (Mulliken) and +0.00007/-0.00003 (NPA), and two P to the C_{60} cages with excess charges of -0.037/-0.032 (Mulliken) and -0.035/-0.031 (NPA). Mulliken-NPA charges and electronic configurations are shown in Table 10. It is seen that NPA electronic structure of the N and P are almost not affected by the encapsulation inside the C_{60} dimers, electronic configurations of two N atoms are $2s^{0.931}\ 2p^{1.888}\ 3s^{1.069}\ 3p^{1.370}$

Table 9: Total energies, E_T, and HOMO-LUMO energy gaps, E_g, of empty C_{60}, $N@C_{60}$ and $P@C_{60}$ dimers for different spin multiplicites.

System	M	E_T(a.u.)	E_g(eV)
C_{60} dimer	1	-4571.1670	2.6158
	3	-4571.1066	1.0052
$N@C_{60}$ dimer	1	-4680.3293	2.5890
	3	-4680.2851	1.9200
$P@C_{60}$ dimer	1	-5253.5781	2.1770
	3	-5253.6049	2.5660

(Gross orbital population) and $2s^{0.931}$ $2p^{1.889}$ $3s^{1.0689}$ $3p^{1.371}$ (Gross orbital population), while NPA electronic configurations are both $2s^{2.00}$ $2p^{3.00}$. Electronic configuration of two P atoms are $3s^{1.357}$ $3p^{1.973}$ $4s^{0.646}$ $4p^{1.101}$ (Gross orbital population) and $3s^{0.09}$ $3p^{0.20}$ $4s^{0.04}$ $4p^{0.05}$ (Gross orbital population), while NPA electronic configurations are $3s^{2.00}$ $3p^{3.03}$ $4s^{0.01}$ and $3s^{2.00}$ $3p^{3.02}$ $4s^{0.01}$.

It can be seen that a part of the HOMO is concentrated on the double C=C bonding sides near the linkage of two C_{60} cages of the singlet $N@C_{60}$ and triplet $P@C_{60}$ dimers in the optimized geometry. LUMO is concentrated inside the left $N@C_{60}$ cage, while it is concentrated in the right C_{60} cage of $P@C_{60}$ dimer. HOMOs of both structures are almost identical to the HOMO of empty C_{60} dimer shown in Figure 15a. Alpha and beta spin density distributions are mainly concentrated on the N and P atoms inside the cages and system's alpha spin density is fully concentrated on left fullerene and beta spin density is fully concentrated on right fullerene for $N@C_{60}$ dimer, while spin density distribution of the right cage consists of partly alpha and beta spins. Figure 17 shows HOMO-LUMO and spin density distributions of $N@C_{60}$ and $P@C_{60}$ dimers.

Table 10: Charges and electronic configurations of N and P inside singlet N@C_{60} and triplet P@C_{60} dimers.

	N-N	P-P
Mulliken Charge	-0.0014,-0.0016	-0.0365,-0.0315
NPA Charge	+0.00007,-0.00003	-0.0351,-0.0305
Gross orbitals	$2s^{0.931}2p^{1.888}3s^{1.069}3p^{1.370}$	$3s^{1.357}3p^{1.973}4s^{0.646}4p^{1.101}$
	$2s^{0.931}2p^{1.889}3s^{1.0689}3p^{1.371}$	$3s^{1.356}3p^{2.000}4s^{0.64647}4p^{1.069}$
NPA	$2s^{2.00}2p^{3.00}$	$3s^{2.00}3p^{3.03}4s^{0.01}$
	$2s^{2.00}2p^{3.00}$	$3s^{2.00}3p^{3.02}4s^{0.01}$

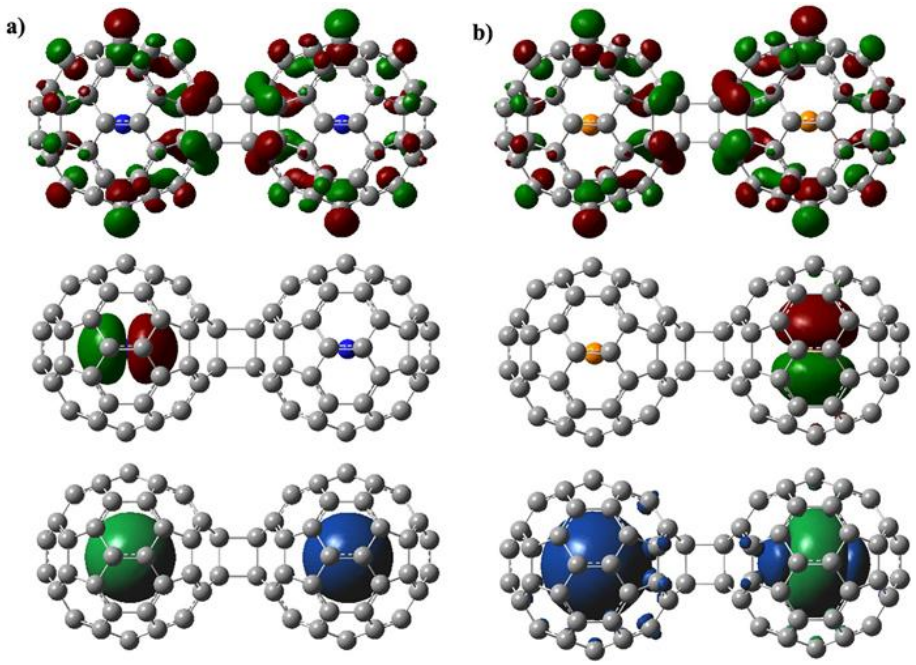

Figure 17: HOMO-LUMO-Spin density graphics of a) N@C_{60} dimer b) P@C_{60} dimer, green and red colors represent positive and negative isosurfaces for HOMO-LUMO, whereas green-blue colors in spin density graphics represent alpha and beta spins.

CHAPTER 6

ELECTRONIC AND GEOMETRICAL STRUCTURE OF METAL AND NON-METAL DOPED C_{60} TRIMERS

6.1 Linear C_{60} Trimers

6.1.1 Li and Na Doped Linear C_{60} Trimers

In this section, three atoms of Li and Na doped linearly [2+2] type bonded three C_{60} fullerene structures are investigated. Bond lengths between three fullerenes are reduced after the encapsulation of metals and Figure 18 shows the optimized bond lengths. Li atoms are located at the center of the cages with Li-Li distances of 9.176-9.125 Å, while Na atoms inside linear Na@C_{60} trimer are not located at the center of the cages.

Off center positions can be seen from the maximum and minimum Na-C distances shown in Table 11. Compared to the positions of Li atoms maximum and minimum distances change, respectively, by 0.36 Å and 0.65 Å in the linear Na@C_{60} trimer. Optimized geometries show that fullerenes at the middle side of the structure extends horizontally and becomes shorter vertically after the encapsulation and four C=C bond formations on the left and right C_{60} cages and eight C=C formations on the middle cage are observed on two hexagons near the linkage sides of three C_{60} cages of empty linear C_{60} trimer just like on the C_{60} dimers in Chapter 5 except that there are eight C=C bonds on the two linkage sides of the middle cage, however optimized geometry of the doublet

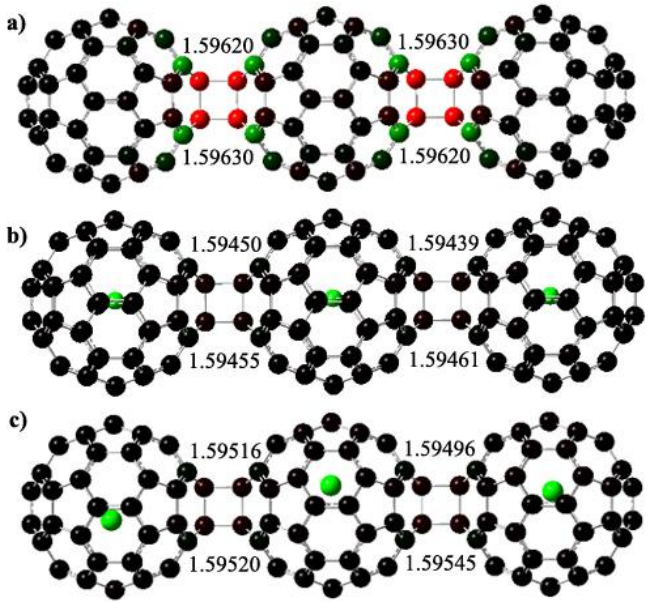

Figure 18: Optimized geometries and charge arrangements of a) Linear C_{60} trimer b) Linear Li@C_{60} trimer and c) Linear Na@C_{60} trimer with given bond distances, red and green colors represent negative and positive charges.

linear Li@C_{60} trimer has only two C=C bonds on left cage, two C=C bonds on the middle cage and three C=C bonds on the right cage located at the linkage sides just like in Figure 14d, while five C=C bond formations occur on linkage sides of the middle cage, two C=C bonds on linkage side of the left cage and two C=C bonds on right cage in the optimized geometry of quartet state of the linear Na@C60 trimer.

Energies of empty linear C_{60}, Li@C_{60}, Na@C_{60} trimers for different spin multiplicities with HOMO-LUMO energy gaps are given in Table 12. Singlet state of empty linear C_{60}, doublet states of linear Li@C_{60} trimer and quartet state of Na@C_{60} trimer are lower in energy. Doublet-quartet energy differences is 0.00272 eV for Li@C_{60} trimer and the same quantity is 0.320 eV for Na@C_{60} trimer. HOMO-LUMO energy separations are, respectively, reduced to 0.7758 eV and 0.8046 eV while empty linear C_{60} trimer has HOMO-LUMO gap of 2.5258 eV.

Table 11: Maximum and minimum distances (in Å) between metals Li-Na and C_{60} cages inside the linear Li@C_{60} and Na@C_{60} trimers.

	Max	Min		Max	Min
Li-C	3.8994	3.3681	Na-C	4.2607	2.7198
	3.9004	3.4249		4.4185	2.7401
	3.8745	3.3912		4.2538	2.7212

Table 12: Total energies, E_T, and HOMO-LUMO energy gaps, E_g, of empty linear C_{60}, Li@C_{60} and Na@C_{60} trimer for different spin multiplicites.

System	M	E_T(a.u.)	E_g(eV)
Empty Linear C_{60}	1	-6856.7451	2.5258
	3	-6856.6855	0.9840
Linear Li@C_{60}	2	-6879.2633	0.8046
	4	-6879.2632	0.7717
Linear Na@C_{60}	2	-7343.6425	0.6699
	4	-7343.6543	0.7758

Mulliken/NPA electron transfers from Li to the C_{60} cages are 1.022/0.831, 1.016/0.833, 1.024/0.831. Same quantities from Na to the C_{60} cages are 0.908/0.838, 0.903/838, 0.908/838. Table 13 shows the Mulliken and NPA charges, and also the corresponding electron configurations. Gross orbital populations for Na and Li atoms show tendency to spread electrons more in upper orbitals, while electrons have tendency to stay in the 1s and 2s orbitals in NPA analysis. It is seen that presence of the interaction between metal atoms Li, Na and C_{60} cages generate charge transfers and so changes the electronic configurations.

Table 13: Charges and electronic configurations of Li and Na inside doublet state of the linear $Li@C_{60}$ and quartet state of $Na@C_{60}$ trimers.

	Li-Li-Li	Na-Na-Na
Mulliken Charge	+1.022,+1.016,+1.024	+0.825,+0.823,+0.828
NPA Charge	+0.831,+0.833,+0.831	+0.869,+0.867,+0.869
Gross orbitals	$2s^{0.05}2p^{0.22}3s^{0.04}3p^{0.26}$	$3s^{0.09}3p^{0.20}4s^{0.04}4p^{0.05}$
	$2s^{0.05}2p^{0.22}3s^{0.04}3p^{0.26}$	$3s^{0.09}3p^{0.21}4s^{0.04}4p^{0.05}$
	$2s^{0.05}2p^{0.22}3s^{0.04}3p^{0.26}$	$3s^{0.09}3p^{0.20}4s^{0.04}4p^{0.05}$
NPA	$2s^{0.13}2p^{0.03}3s^{0.01}3p^{0.01}$	$3s^{0.11}3p^{0.01}4s^{0.01}$
	$2s^{0.12}2p^{0.03}3s^{0.01}3p^{0.01}$	$3s^{0.11}3p^{0.01}4s^{0.01}$
	$2s^{0.13}2p^{0.03}3s^{0.01}3p^{0.01}$	$3s^{0.11}3p^{0.01}4s^{0.01}$

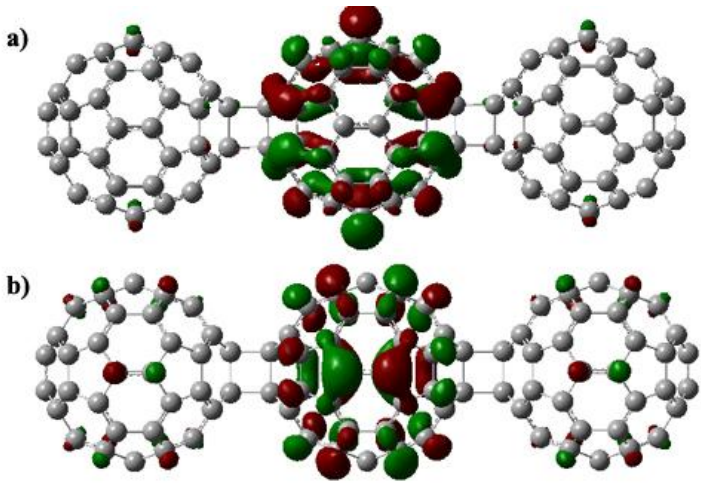

Figure 19: HOMO and LUMO graphics of empty linear C_{60} trimer of linear empty C_{60} trimer a) HOMO b) LUMO, green and red colors represent positive and negative isosurfaces.

Spin densities of linear Li@C_{60} and Na@C_{60} trimers are mainly distributed around the C_{60} cages. In linear Li@C_{60} trimer, compared to the empty C_{60} trimer's HOMO and LUMO which are localized around the middle cage shown in Figure 19, HOMO is concentrated on the right side of the trimer, while LUMO is distributed equally around the C_{60} cages. HOMO states of quartet Na@C_{60} trimer distributed mainly around the two right cages, while LUMO is distributed equally around the C_{60} cages. Figure 20 shows the HOMO-LUMO and spin density distributions.

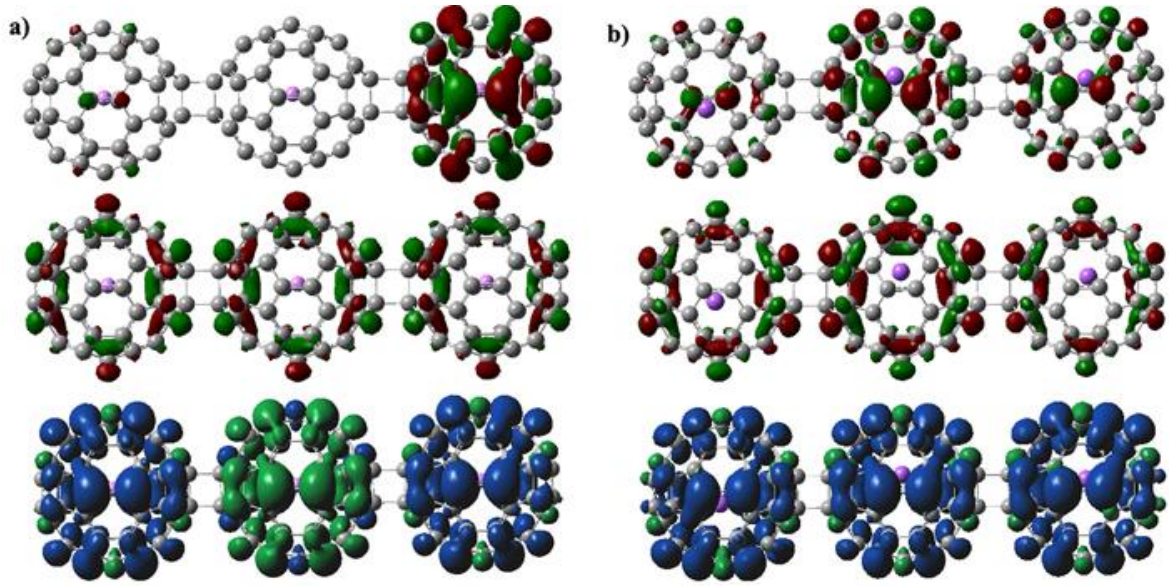

Figure 20: HOMO-LUMO orbital graphics and spin densities of a) linear Li@C_{60} trimer b) linear Na@C_{60} trimer, green and red colors represent the positive and negative isosurfaces of HOMO-LUMO, whereas green-blue colors of spin density graphics represent alpha and beta spins.

6.1.2 N and P Doped Linear C_{60} Trimers

Optimized geometries of linear $N@C_{60}$ and $P@C_{60}$ trimers show that three non-metal atoms of N and P are located almost at the center of the cages. Charge arrangements of the N and P doped systems with bond lengths and maximum-minimum N-C and P-C distances are given in Figure 21 and Table 14.

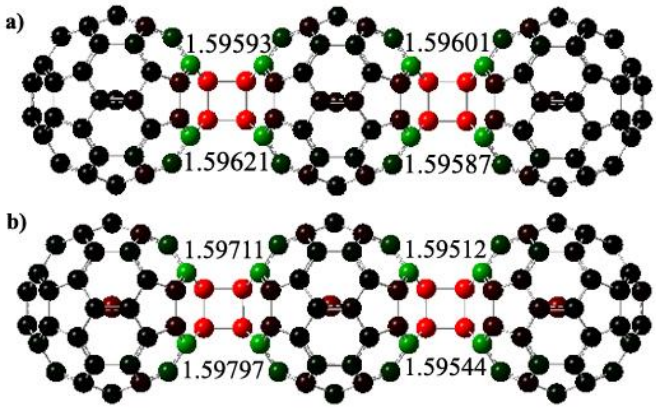

Figure 21: Optimized geometries and charge arrangements of a) Linear $N@C_{60}$ trimer and b) Linear $P@C_{60}$ trimer with given bond distances, green and red colors represent positive and negative charges.

Distances between three N atoms are 9.14 -9.09 Å and P atoms are 9.00-9.36 Å in the optimized geometries. Maximum and minimum distances show that fullerenes at the middle side of the structures extends horizontally and becomes shorter vertically and double C=C bond formations, four C=C on the left cage, eight C=C on the middle cage and four C=C on the right cage, are observed on two hexagons near the linkage sides of three C_{60} cages of quartet $N@C_{60}$ and $P@C_{60}$ trimers which are exactly the same bond

formations as on the singlet empty C_{60} trimer in Chapter 6.1.1. Compared to metal doped linear trimers, there is no change in double bond formations after non-metal doping.

Table 14: Maximum and minimum distances (in Å) between metals N-P and C_{60} cages inside the linear N@C_{60} and P@C_{60} trimers.

	Max	Min		Max	Min
N-C	3.9031	3.5054	P-C	3.8880	3.4108
	3.9167	3.4818		4.0358	3.3911
	3.7660	3.4326		3.9264	3.4438

Energies of empty linear C_{60}, linear N@C_{60}, P@C_{60} trimers with different spin multiplicities and HOMO-LUMO energy gaps are given in Table 15. Singlet state of empty linear C_{60} and quartet states of linear N@C_{60} and P@C_{60} trimers are lower in energy with the energy gap of 0.001 eV and 0.7733 eV, respectively. HOMO-LUMO energy gap is lowest in doublet P@C_{60} trimer.

Mullilken/NPA, electron transfers from the C_{60} cages to the N atoms are 0.001357/0.00011, 0.007030/0.00410, 0.004597/0.00351. The same quantities from C_{60} cages to the P atoms are 0.0323/0.0311, 0.0356/0.0335, 0.0318/0.0306. It can be seen that presence of low interactions between atoms and the cages preserve electronic configurations of the atoms. Table 16 shows the excess charge and electronic configurations of the structures.

Table 15: Total energies, E_T, and HOMO-LUMO energy gaps, E_g, of empty linear C_{60}, $N@C_{60}$ and $P@C_{60}$ trimers for different spin multiplicites.

System	Multiplicity	E_T(a.u)	E_g(eV)
Empty Linear C_{60}	1	-6856.7451	2.5258
	3	-6856.6855	0.9840
Linear $N@C_{60}$	2	-7020.3998	1.8503
	4	-7020.3999	1.2281
Linear $P@C_{60}$	2	-7880.4106	2.1312
	4	-7880.4390	2.5200

Table 16: Charges and electronic configurations of N and P inside quartet linear $N@C_{60}$ and $P@C_{60}$ trimers.

	N-N-N	P-P-P
Mulliken Charge	-0.001357,-0.007030,-0.004597	-0.0323,-0.0356,-0.0318
NPA Charge	-0.00011,-0.00410,-0.00351	-0.0311,-0.0335,-0.0306
Gross orbitals	$2s^{0.95}2p^{1.93}3s^{1.06}3p^{1.08}$	$3s^{1.360}3p^{1.9996}4s^{0.647}4p^{1.070}$
	$2s^{0.95}2p^{1.89}3s^{1.05}3p^{1.12}$	$3s^{1.356}3p^{2.001}4s^{0.647}4p^{1.073}$
	$2s^{0.95}2p^{1.89}3s^{1.05}3p^{1.11}$	$3s^{1.356}3p^{1.9993}4s^{0.647}4p^{1.070}$
NPA	$2s^{2.00}2p^{3.00}$	$3s^{2.00}3p^{3.02}4s^{0.01}$
	$2s^{2.00}2p^{3.00}$	$3s^{2.00}3p^{3.03}4s^{0.01}$
	$2s^{2.00}2p^{3.00}$	$3s^{2.00}3p^{3.02}4s^{0.01}$

Spin densities of linear $N@C_{60}$ and $P@C_{60}$ trimers are inside the C_{60} cages but with different alpha and beta distributions. HOMO of $N@C_{60}$ trimer is distributed around the middle cage and LUMO is inside that cage. However, in linear $P@C_{60}$ trimer LUMO is concentrated around the middle C_{60} cage while HOMO is identical to HOMO of the linear $N@C_{60}$ trimer. Both structures' HOMOs are almost identical HOMO of the empty linear C_{60} trimer and LUMO of linear $P@C_{60}$ trimer is almost identical to LUMO of the empty linear C_{60} trimer shown in Figure 19. Figure 22 shows the HOMO-LUMO and spin density distributions.

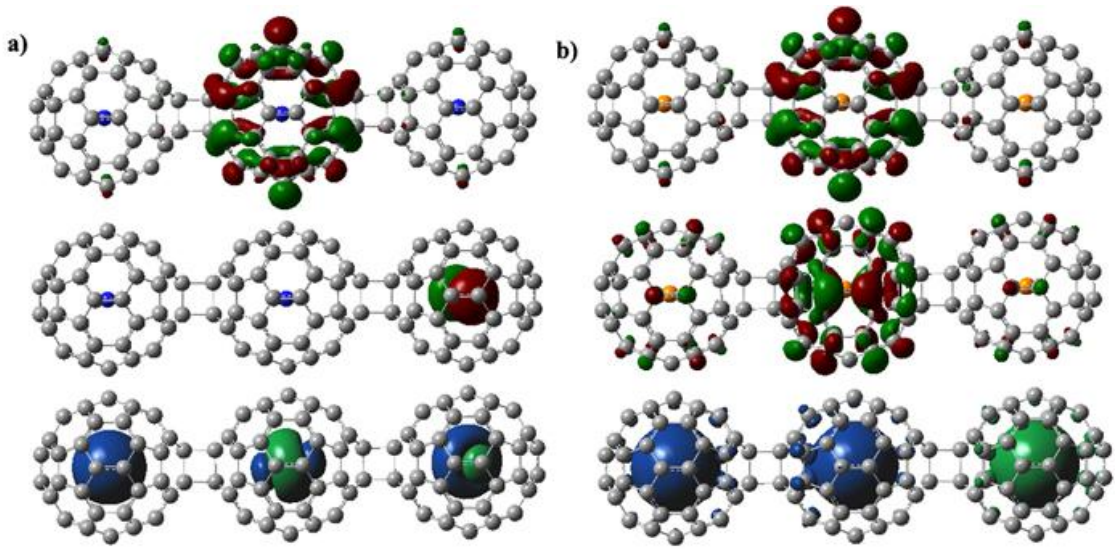

Figure 22: HOMO-LUMO orbital graphics and spin density of a) linear $N@C_{60}$ trimer b) linear P@C60 trimer, green and red colors represent the positive and negative isosurfaces of HOMO LUMO, whereas and green-blue colors in spin density graphics represent alpha and beta spins.

6.2 Triangular C_{60} Trimers

6.2.1 Li and Na Doped Triangular C_{60} Trimers

Li and Na doped triangular C_{60} trimers consist of three C_{60} fullerenes linked by [5+5] type C-C bonds. Bond lengths of the empty triangular C_{60}, $Li@C_{60}$ and $Na@C_{60}$ trimers are given in Table 17 and maximum/minimum Li-C and Na-C distances are in Table 18.

Table 17: [5+5] bond lengths of triangular singlet C_{60}, quartet $Li@C_{60}$ and doublet $Na@C_{60}$ trimers in Å.

	$a_{1,2,3,4,5}$	$b_{1,2,3,4,5}$	$c_{1,2,3,4,5}$
Triangular C_{60}	1.61100	1.61092	1.61078
	1.61058	1.61058	1.61110
	1.61317	1.61317	1.61373
	1.61306	1.61306	1.61277
	1.57213	1.57214	1.57204
Triangular $Li@C_{60}$	1.62168	1.62419	1.62089
	1.62561	1.61906	1.62344
	1.61845	1.61703	1.61515
	1.61757	1.61735	1.61737
	1.57289	1.57310	1.57306
Triangular $Na@C_{60}$	1.62669	1.62658	1.64933
	1.62604	1.62627	1.64962
	1.61652	1.61668	1.62140
	1.61687	1.61720	1.61904
	1.57228	1.57224	1.57206

After encapsulation of metals $a_{1,2}$, $b_{1,2}$ and $c_{1,2}$ bond lengths shown in Figure 23d are reduced by 0.01 Å . It can be seen from the max./min. distances that Li atoms are not located at the center of the cages in the optimized geometry of quartet triangular Li@C_{60} trimer and their off center positions change about 1 Å compared to triangular Na@C_{60} trimer.

Table 18: Maximum and minimum distances between metals Li-Na and C_{60} cages inside the triangular Li@C_{60} and Na@C_{60} trimers in Å.

	Max	Min		Max	Min
Li-C	5.11861	2.19394	Na-C	3.93138	3.48541
	4.93239	2.16092		3.86043	3.47962
	5.03344	2.20454		3.75157	3.38022

Mulliken charge arrangements of the empty C_{60} is different from NPA charge arrangements in such a way that five carbon atoms in the [5+5] type bonded C-C linkage sides are negatively charged and hexagon sides of the three fullerene cages have two extra negatively charged atoms. Mulliken and NPA charge arrangements are given in Figure 23.

Energies and HOMO-LUMO gaps of the Li-Na doped triangular systems are given in Table 19. Calculated total energies show that energy of quartet state of triangular Li@C_{60} is lower than doublet state with an energy separation of 1.6055 eV. However same situation is not valid for triangular Na@C_{60}, its doublet state is lower than quartet state with energy separation of 0.0708 eV. HOMO-LUMO energy gap of quartet state of triangular Li@C_{60} trimer is higher than the HOMO-LUMO energy gap of doublet state

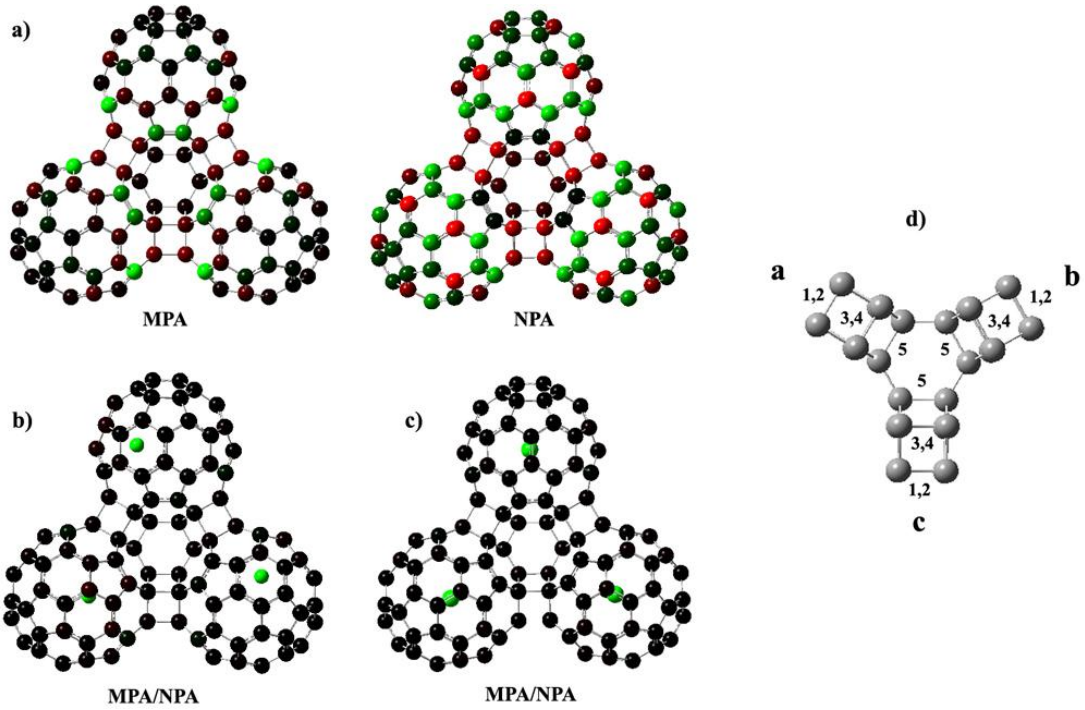

Figure 23: Optimized geometry and charge arrangements of triangular C_{60} trimer; a) Mulliken and NPA charge arrangements of C_{60} b) Mulliken/NPA charge arrangements of quartet state of triangular $Li@C_{60}$ trimer c) Mulliken/NPA charge arrangements of doublet state of triangular $Na@C_{60}$ trimer d) [5+5] type bonds represented by $a_{1,2,3,4,5}$, $b_{1,2,3,4,5}$ and $c_{1,2,3,4,5}$, green and red colors represent positive and negative charges.

of linear $Li@C_{60}$ trimer, while doublet state of triangular $Na@C_{60}$ trimer has lower HOMO-LUMO energy gap than quartet state of linear $Na@C_{60}$ trimer which is lower in total energy. Mulliken/NPA, electron transfer from Li atoms to the C_{60} cages are 0.637/0.868, 0.633/0.871, 0.616/0.867. The same quantities from Na to the C_{60} cages are 0.8805/0.8321, 0.8769/0.8275, 0.8763/0.8270. Final electronic configurations of Na inside the trimer show that remaining valence electrons stay in the 3p-4p orbitals according to Mulliken analysis and 3s orbital according to NPA. Electronic configurations and excess charges are given in Table 20.

Table 19: Total energies, E_T, and HOMO-LUMO energy gaps, E_g, of singlet triangular C_{60}, quartet Li@C_{60} and doublet Na@C_{60} trimers for different spin multiplicities.

System	Multiplicity	E_T(a.u)	E_g(eV)
Triangular C_{60}	1	-6856.2449	1.1881
	3	-6856.2304	1.0087
Triangular Li@C_{60}	2	-6878.8326	0.6588
	4	-6878.8916	0.9192
Triangular Na@C_{60}	2	-7343.2036	0.6427
	4	-7343.2010	0.7314

Table 20: Charges and electronic configurations of Li and Na inside doublet triangular Li@C_{60} and Na@C_{60} trimers.

	Li-Li-Li	Na-Na-Na
Mulliken Charge	+0.637,+0.633,+0.616	0.8805,+0.8769,+0.8763
NPA Charge	+0.868,+0.871,+0.867	+0.8321,+0.8275,+0.8270
Gross orbitals	$2s^{0.120}2p^{0.330}3s^{0.014}3p^{0.07}$	$3s^{0.084}3p^{0.201}4s^{0.048}4p^{0.108}$
	$2s^{0.114}2p^{0.336}3s^{0.015}3p^{0.07}$	$3s^{0.074}3p^{0.201}4s^{0.048}4p^{0.108}$
	$2s^{0.120}2p^{0.346}3s^{0.012}3p^{0.07}$	$3s^{0.076}3p^{0.190}4s^{0.048}4p^{0.108}$
NPA	$2s^{0.10}2p^{0.02}3s^{0.01}3p^{0.01}$	$3s^{0.14}3p^{0.02}4s^{0.01}$
	$2s^{0.10}2p^{0.02}3p^{0.01}$	$3s^{0.14}3p^{0.02}4s^{0.02}$
	$2s^{0.09}2p^{0.02}3s^{0.01}3p^{0.01}$	$3s^{0.14}3p^{0.02}4s^{0.02}$

HOMO and LUMO are given in Figure 24. HOMO of triangular Li@C_{60} trimer has a different distribution on the cages than triangular Na@C_{60} trimer, both HOMO and LUMO are concentrated on the left cages of triangular Li@C_{60}. On the other hand,

Figure 24b shows that HOMO of triangular Na@C_{60} is distributed around the lower two cages and LUMO is on the upper cage.

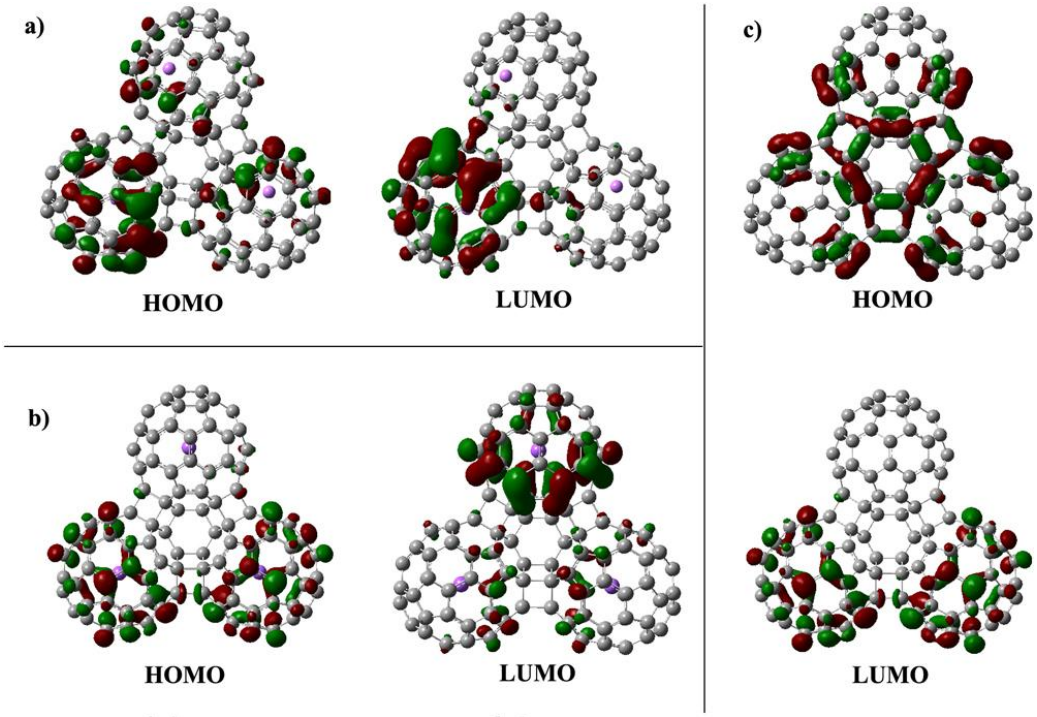

Figure 24: HOMO-LUMO orbital graphics of a) quartet triangular Li@C_{60} b) doublet triangular Na@C_{60} c) Singlet triangular C_{60} trimer, green and red colors represent the positive and negative isosurfaces.

Spin densities of both structures are around the fullerene sides. However, spin distribution of the quartet state of the triangular Li@C_{60} is around all three fullerenes while spin density is around the upper cage in triangular Na@C_{60} trimer. Spin density distributions are given in Figure 25.

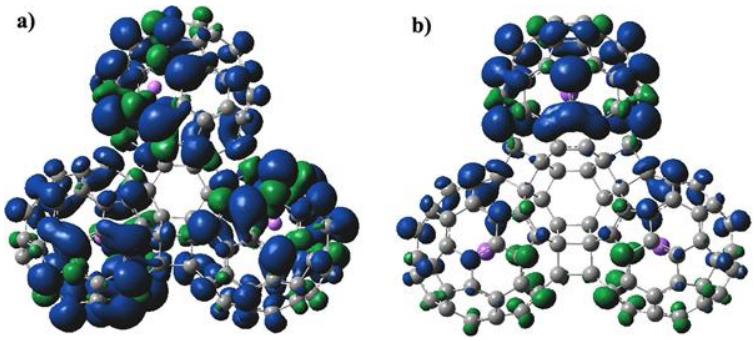

Figure 25: Spin densities of triangular Li@C_{60} and Na@C_{60}, green-blue colors represent alpha and beta spins.

6.2.2 N and P Doped Triangular C_{60} Trimers

In this section, structures of three N and P doped trimers are investigated. Optimized geometries with charge arrangements are given in Figure 26. Both N and P atoms are located at the center of the C_{60} cages. [5+5] bond lengths and maximum-minimum N-C and P-C distances are given in Tables 21-22.

Carbon [5+5] bond lengths are almost not changed, vary between 0.001 Å and 0.0005 Å, compared to the [5+5] bonds of metal doped trimers. It is seen that quartet states of triangular N@C_{60} and P@C_{60} trimers are lower in energy and separated from the doublet state by 0.381 eV and 0.737 eV. Total energies and HOMO-LUMO energy gaps are given in Table 23. Both quartet states have HOMO-LUMO gap near 1 eV.

Mulliken/NPA, electron transfer from N atoms to the C_{60} cages are -0.00344/ -0.00204, -0.00477/ -0.00337, -0.00434/ -0.00294. The same quantities from P to the C_{60} cages are -0.02946/ -0.02123, -0.02942/ -0.02115, -0.02955/ -0.02144. Like in the N and P doped dimer and linear trimer structures, it can be seen that presence of low interactions between atoms and the cages preserve electronic configurations of the atoms. Electronic configurations and excess charges are given in Table 24.

Table 21: [5-5] bond lengths of triangular singlet C_{60}, quartet $N@C_{60}$ and quartet $P@C_{60}$ trimers in Å.

	$a_{1,2,3,4,5}$	$b_{1,2,3,4,5}$	$c_{1,2,3,4,5}$
Triangular C_{60}	1.61100	1.61092	1.61078
	1.61058	1.61058	1.61110
	1.61317	1.61317	1.61373
	1.61306	1.61306	1.61277
	1.57213	1.57214	1.57204
Triangular $N@C_{60}$	1.61053	1.61043	1.61093
	1.61051	1.61028	1.61116
	1.61395	1.61430	1.61519
	1.61440	1.61487	1.61375
	1.57192	1.57185	1.57187
Triangular $P@C_{60}$	1.61092	1.61083	1.61169
	1.61085	1.61068	1.61187
	1.61369	1.61361	1.61565
	1.61454	1.61392	1.61315
	1.57256	1.57258	1.57217

Table 22: Maximum and minimum distances (in Å) between non-metals N-P and C_{60} cages inside the triangular $N@C_{60}$ and $P@C_{60}$ trimers.

Max	Min		Max	Min
N-C 3.86532	3.44213	P-C	3.78772	3.46916
3.96440	3.46532		3.78589	3.45778
3.81035	3.50850		3.81182	3.48266

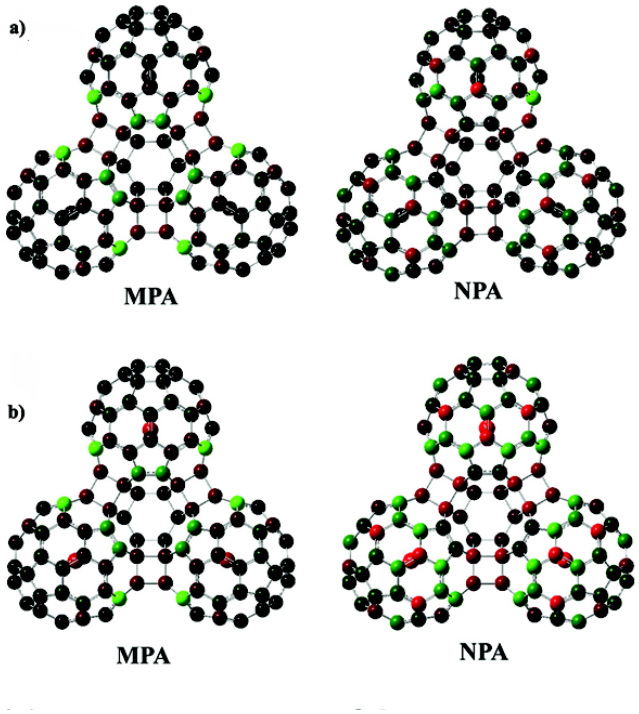

Figure 26: Optimized geometries and MPA/NPA charge arrangements of a) triangular N@C_{60} trimer b) triangular P@C_{60} trimer, red and green colors represent negative and positive charges.

Table 23: Total energies, E_T, and HOMO-LUMO energy gaps, E_g, of triangular C_{60}, N@C_{60} and P@C_{60} trimers for different spin multiplicites (M).

System	M	E_T(a.u.)	E_g(eV)
Triangular C_{60}	1	-6856.2449	1.1881
	3	-6856.2304	1.0087
Triangular N@C_{60}	2	-7019.9758	1.0836
	4	-7019.9898	1.1556
Triangular P@C_{60}	2	-7879.9196	1.1549
	4	-7879.9510	1.1527

Table 24: Charges and electronic configurations of N and P inside quartet triangular $N@C_{60}$ and $P@C_{60}$ trimers.

	N-N-N	P-P-P
Mulliken Charge	-0.00344,-0.00477,-0.00434	-0.02946,-0.02942,-0.02955
NPA Charge	-0.00204,-0.00337,-0.00294	-0.02123,-0.02115,-0.02144
Gross orbitals	$2s^{0.93}2p^{1.929}3s^{1.060}3p^{1.07}$	$3s^{1.36}3p^{1.996}4s^{0.643}4p^{1.070}$
	$2s^{0.95}2p^{1.932}3s^{1.053}3p^{1.083}$	$3s^{1.36}3p^{1.996}4s^{0.643}4p^{1.071}$
	$2s^{0.95}2p^{1.844}3s^{1.054}3p^{1.083}$	$3s^{1.36}3p^{1.995}4s^{0.643}4p^{1.071}$
NPA	$2s^{2.00}2p^{3.00}$	$3s^{2.00}3p^{3.02}4s^{0.01}$
	$2s^{2.00}2p^{3.00}$	$3s^{2.00}3p^{3.01}4s^{0.01}$
	$2s^{2.00}2p^{3.00}$	$3s^{2.00}3p^{3.02}4s^{0.01}$

HOMOs of triangular $N@C_{60}$ and $P@C_{60}$ trimers are concentrated on the linkage sides of the C_{60} cages and LUMOs are concentrated on the right cage. Figure 27 shows HOMO-LUMO of triangular $N@C_{60}$ and $P@C_{60}$ trimers. Both structures show almost identical HOMO-LUMO distributions to empty C_{60} as shown in Figure 24c.

The spin density distribution of the N doped triangular trimer is shown in Figure 28. Most of the spin resides on the N atom (inside the cages). In doublet state of the $N@C_{60}$ trimer, spin density of the two N doped C_{60} parts have their spin densities inside the C_{60} cages but the third one is not exactly inside the cage with its all parts. However, the spin density of the quartet state of $N@C_{60}$ trimer is fully inside the cage. Figure 28 shows this comparison.

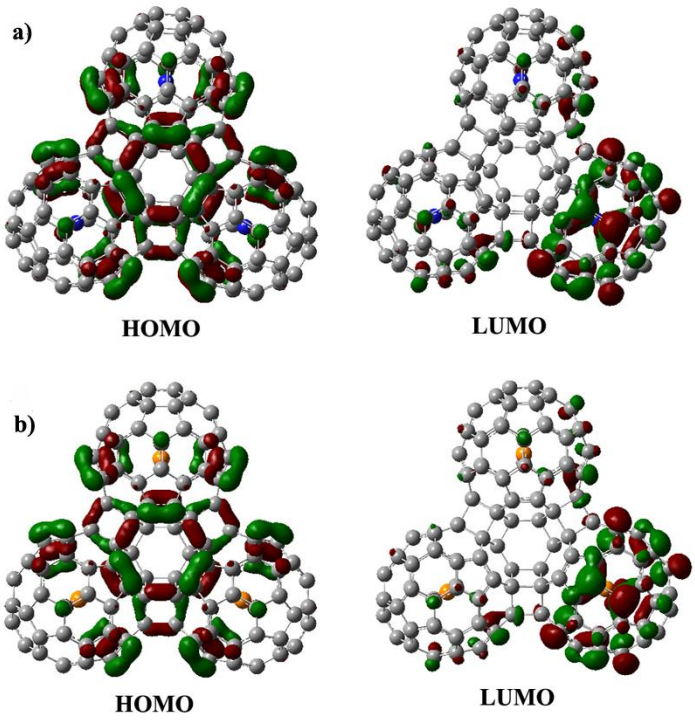

Figure 27: HOMO, LUMO graphics of quartet triangular $N@C_{60}$ and doublet triangular $P@C_{60}$ trimers. a) HOMO, LUMO of $N@C_{60}$, b) HOMO, LUMO of $P@C_{60}$. Green and red color represent the positive and negative isosurfaces, respectively.

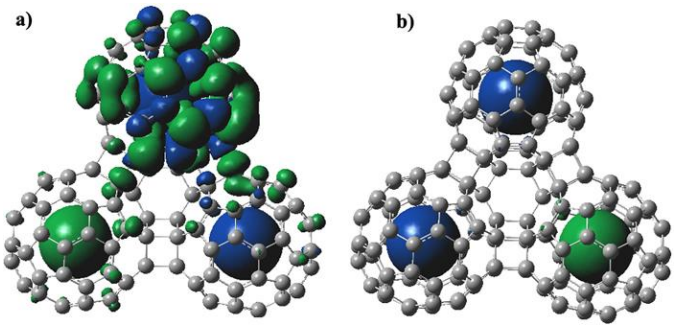

Figure 28: Spin density distributions of a) doublet state of triangular $N@C_{60}$ trimer, b) quartet state of triangular $N@C_{60}$ trimer. Green, blue colors represent alpha and beta spins, respectively.

Spin distributions of both doublet and quartet states of P doped trimer are inside the C_{60} cages. The upper $P@C_{60}$ cage of the doublet state consists of alpha and beta spin distributions while the spin density distribution of the upper part of the quartet state of triangular $P@C_{60}$ trimer is fully consists of beta spin. These results are shown in Figure 29.

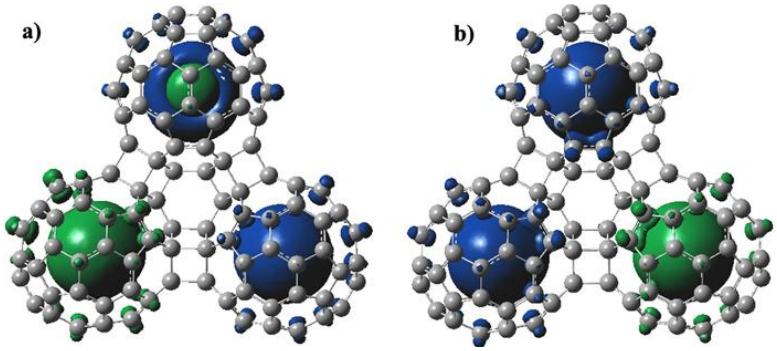

Figure 29: Spin density distributions of a) doublet state of triangular $P@C_{60}$ trimer, b) quartet state of triangular $P@C_{60}$ trimer. Green, blue colors represents alpha and beta spins, respectively.

CHAPTER 7

CONCLUSION

Number of studies on the subject of quantum information and computation including experimental and theoretical studies grow very fast and there are already many proposals of quantum computers some of them are mentioned in this study. Taking into account the DiVincenzo criteria, the main aim of this thesis is to investigate the spin-qubit properties of different fullerene structures using DFT calculations by giving the charge transfer mechanism, electronic configurations and spin density distributions. Based on the requirements of DiVincenzo[82] and its adapted version for molecular spin-qubits[54] which consists of nature and mechanism of interaction and charge and spin distributions, little work has been done using ab-initio studies to investigate this spin-qubit properties of molecular structures by looking at nature of the interactions some of which are referenced in this thesis. Hovewer, the studies, investigating charge-spin distribution and electronic configurations of metal and nonmetal doped dimer and trimer fullerene structures using density functional theory in order to find a suitable spin-qubit condidates, given in this thesis is probably the first study in this field.

In this thesis, electronic structure calculations of metal (Li,Na) and non-metal (N,P) doped C_{60} dimers and trimers are carried out using hybrid density functional theory in order to investigate the spin-qubit properties by giving spin density distributions, charge arrangements and electronic configurations. Spin densities of the metal doped structures are around the fullerene sides and presence of an interaction between the metal atoms and the cages does change the electronic configurations and charge transfer occurs between metal atoms and C_{60} cages, it is from metal atoms to the cages, so they might be tested inside nanotube structures to study the function of the nanotube. Optimized

structures of linear C_{60} trimers are more stable than triangular trimers, i.e. their total energy is lower than triangular trimers and the most stable configuration of triangular ones are not doublet states except for $Na@C_{60}$. Spin densities of non-metal doped structures are mainly inside the cages and there is no significant charge transfer between non-metal atoms and the C_{60} cages therefore electronic configurations become unchanged.

Protected spins and electronic configurations and low charge transfer between carbon cages and non-metal atoms N and P inside the fullerene-based structures (based on the results given in this thesis studies) are desired structures for a well defined spin qubit because a quantum computer's units must be well isolated from the environment and carbon cages in the studied structures provides a good isolation against the environment for the non-metal atoms N and P. These results are also supported by previously studied long decoherence times of N and P doped fullerenes [197-199]. In addition, we think that calculated HOMO-LUMO orbitals can be used to determine the type of experimental operations that is planned to use in manipulations of spin-qubits in solid state quantum computer proposals. Recently, there are studies to investigate the interactions, manipulations, electronic structures, transport properties and characterization of quantum dots in triangular configuration as spin-qubits and qutrits [206-213]. We hope that calculated electronic structures, spin density distributions and energy differences for different spin configurations of the metal and non-metal doped C_{60} chains can be helpful to study the designing of special spintronic devices including spin cluster qubits and qutrits of doped triangular C_{60} trimers in fullerene based quantum computer proposals.

The numerical calculations reported in this thesis were performed at TUBITAK ULAKBIM, High Performance and Grid Computing Center (TR-Grid e-Infrastructure) and based on the studies and the idea depicted in this thesis, there are two articles have been planned to to be published; one article called "*Investigation of metal and non-metal doped dimer and trimer C_{60} fullerene chains as prospective spin cluster qubits*" is prepared and submitted.

REFERENCES

1. N. Taniguchi, *On the Basic Concept of 'Nano-Technology'*, Proc. Intl. Conf. Prod. Eng. Tokyo, Part II, Japan Society of Precision Engineering, 1974.

2. R. P. Feynman, Engineering and Science **23**, 22 (1960).

3. R. Brazil, Nanotechnology-The Issues, www.rsc.org/pdf/policy/nanotechnology.pdf; Last visited 26/05/2010.

4. R. Paull, J. Wolfe, P. Hebert and M. Sinkula, Nat. Biotechnol. **21 (10)**, 1144 (2003).

5. M. C. Roco and W.S. Bainbridge, Nanoscale Science, Engineering and Technology (NSET) workshop report, Societal Implication of Nanoscience and Nanotechnology, http://www.wtec.org/loyola/nano/NSET.Societal.Implications/nanosi.pdf; Last visited 26/05/2010.

6. R. C. Johnson, Nanotech R&D Act Becomes Law, EE Times, http://www.eetimes.com/story/OEG20031203S0025; Last visited 26/05/2010.

7. W. Jeffrey, Importance of Basic Research to United States' Competitiveness, National Institute of Standards and Technology (NIST), http://www.nist.gov/director/ocla/testimony/loader.cfm?csModule=security/getfile&pageid=1261898; Last visited 26/05/2010.

8. W. L. Greaves-Holmes, J. Tech. Stud. [Online] **35** (1), 33 (2009). http://scholar.lib.vt.edu/ejournals/JOTS/v35/v35n1/pdf/holmes.pdf; Last visited 26/05/2010.

9. Nano Patents and Innovations, http://nanopatentsandinnovations.blogspot.com/2010/01/2009-record-year-for-nanotechnology.html; Last visited 26/05/2010.

10. H. B. Gray, *Chemical bonds; an introduction to atomic and molecular structure*, (Menlo Park, Calif., W. A. Benjamin 1973).

11. M. J. O'Connell, *Carbon nanotubes: properties and applications*, (Boca Raton, FL : CRC/Taylor & Francis, 2006).

12. R. Saito, G. Dresselhaus and S. Dresselhaus, *Physical properties of carbon nanotubes,* (London : Imperial College Press , 1998).

13. S. Iijima, Nature **354**, 56 (1991).

14. H. W. Kroto, J. R. Heath, S. C. O'Brien, R. F. Curland, R. E. Smalley, Nature **318**, 162 (1985).

15. H. Yamaoka, H. Sugiyama, Y. Kubozono, A. Kotani, R. Nouchi, A. M. Vlaicu, H. Oohashi, T. Tochio, Y. Ito, and H. Yoshikawa, Phys. Rev. B **80**, 205403 (2009).

16. Z. C. Ying, J. G. Zhu, R. N. Compton , L. F. Allard, R. L. Hettich, and R. E. Haufler, Synthesis of Doped Fullerene Clusters and Boron-Nitrogen Tubules Using Laser Ablation, Vairavamurthy, M.A.; Schoonen,M. A. A., Eds.; ACS Symposium Series 679; American Chemical Society: Washington, DC, 1997, 169–182.

17. H. Shinohara, Rep. Prog. Phys. **63**, 843 (2000).

18. Y. Yun, V. Shanov, Y. Tu, M. J. Schulz, Se. Yarmolenko, S. Neralla, J. Sankar, and S. Subramaniam, *Nano Lett.* **6**, 689 (2006).

19. S. Okada, Phys. Rev. B **72**, 153409 (2005).

20. T. W. Chamberlain, A. Camenisch, N. R. Champness, G. A. D. Briggs, S. C. Benjamin, A. Ardavan, and A. N. Khlobystov, J. Am. Chem. Soc. **129**, 8609 (2007).

21. A. Loiseau, *Understanding carbon nanotubes: from basics to applications,* (Berlin, Heidelberg : Springer, 2006).

22. J. S. Kilby , IEEE T. Electron Dev. **23**, 648 (1976).

23. G. E. Moore, Electronics **38 (8)**, 114 (1965).

24. R. P. Feynman, Int. J. Theor. Phys. **21**, 467 (1982).

25. R. P Feynman Opt. News **11**, 11 (1985).

26. S. Wiesner, Sigact News, **15**, 78 (1983).

27. C. H. Bennett and G. Brassard, "Quantum Cryptography: Public key distribution and coin tossing", Proceedings of the IEEE International Conference on Computers, Systems, and Signal Processing, Bangalore, 175 (1984).

28. A. K. Ekert, Phys. Rev. Lett. **67**, 661 (1991).

29. N. Gisin, G. Ribordy, H. Zbinden, D. Stucki, N. Brunner and V. Scarani, ", arXiv:quant-ph/0411022, arXiv.org e-Print archive. http://arxiv.org/abs/quant-ph/0411022 (2004). Last visited 26/05/2010.

30. K. Inoue, E. Waks and Y. Yamamoto, Phys. Rev. Lett. **89**, 037902 (2002).

31. E. H. Serna, *Quantum Key Distribution Protocol with Private-Public Key*, arXiv:0908.2146v3, arXiv.org e-Print archive. http://arxiv.org/abs/0908.2146 (2009). Last visited 26/05/2010.

32. D. Deutsch, Proc. Roy. Soc. London A **400**, 97 (1985).

33. D. Deutsch and R. Jozsa, Proc. Roy. Soc. London A **439**, 553 (1992).

34. P.W. Shor, SIAM J. Sci. Statist. Comput. **26**, 1484 (1997).

35. L. M. K. Vandersypen, M. Steffen, G. Breyta, C. S. Yannoni, M. H. Sherwood and I. L. Chuang, *Nature* **414**, 883 (2001).

36. L. K. Grover, *A fast quantum mechanical algorithm for database search,* Proc. 28th annual ACM STOC, 212-219 (1996), arXiv:0908.2146v3.

37. D. R. Simon, *On the power of quantum computation*, Proc. 35th Annual Symposium on Foundations of Computer Science, edited by S. Goldwasser (IEEE Computer Society, Los Alamitos, CA, 1994), pp.116-123.

38. D-Wave Systems, http://dwave.wordpress.com/2007/01/19/quantum-computing-demo-announcement/. Last visited 26/05/2010.

39. D-Wave Systems, http://dwave.wordpress.com/2008/12/19/. Last visited 26/05/2010.

40. T. Schmitt-Manderbach, H. Weier, M. Fürst, R. Ursin, F. Tiefenbacher, T. Scheid, J. Perdigues, Z. Sodnik, C. Kurtsiefer, J. G. Rarity, A. Zeilinger, and H. Weinfurter, Phys. Rev. Lett**. 98**, 010504 (2007).

41. M. Toyoshima, Y. Takayama, W. Klaus, H. Kunimori, M. Fujiwara and M. Sasaki, Acta Astronaut. **63**, 179 (2008).

42. A. Tanaka et al. Opt. Express **16**, 11354 (2008).

43. T. Kimura, Y. Nambu, T. Hatanaka, A. Tomita, H. Kosaka, and K. Nakamura, Jpn. J. Appl. Phys. **43**, 1217 (2004).

44. C. Gobby, Z. L. Yuan, and A. J. Shields, Appl. Phys. Lett. **84**, 376 (2004).

45. A. Tajima, A. Tanaka, W. Maeda, S. Takahashi, and A. Tomita, IEEE J. Sel. Top. Quantum Electron. **13**, 1031 (2007).

46. D. Stucki, N. Walenta, F. Vannel, R. T. Thew, N. Gisin, H. Zbinden, S. Gray, C. R. Towery and S. Ten, New J. Phys. **11**, 075003 (2009).

47. C. Erven, C. Couteau, R. Laflamme, and G. Weihs, Opt. Express 16, 16840 (2008).

48. P. Villoresi, T. Jennewein, F. Tamburini, M. Aspelmeyer, C. Bonato, R. Ursin, C. Pernechele, V. Luceri, G. Bianco, A. Zeilinger and C. Barbieri, *New J. Phys*. **10**, 033038 (2008).

49. B. P. Lanyon, J. D. Whitfield, G. G. Gillett, M. E. Goggin, M. P. Almeida, I. Kassal, J. D. Biamonte, M. Mohseni, B. J. Powell, M. Barbieri, A. Aspuru-Guzik and A. G. White. Nature Chemistry **2**, 106 (2010).

50. M.A. Nielsen and I. L. Chuang, *Quantum computation and quantum information,* (Cambridge ; New York : Cambridge University Press, 2000).

51. M. Lanzagorta and J. Uhlmann, *Quantum computer science,* (San Rafael, Calif.: Morgan & Claypool Publishers, c2009).

52. P. Kaye, R. Laflamme, M. Mosca, *An introduction to quantum computing,* (Oxford : Oxford University Press, 2007).

53. G. P. Berman et al., *Introduction to quantum computers,* **(**Singapore; River Edge, N.J. : World Scientific, c1998).

54. D. McMahon, *Quantum computing explained,* (Hoboken, N.J.: Wiley-Interscience : IEEE Computer Society, c2008.)

55. M. Hirvensalo, *Quantum computing,* (New York: Springer, 2001).

56. M. Fox, *Quantum optics : an introduction,* (Oxford ; New York: Oxford University Press, 2006).

57. A. O. Pittenger, *An introduction to quantum computing algorithms***, (**Boston: Birkhauser, 1999).

58. N. David Mermin, *Quantum computer science : an introduction,* (Cambridge: Cambridge University Press, 2007).

59. J. Stolze and D. Suter, *Quantum computing : a short course from theory to experiment*, (Weinheim: Wiley-VCH, c2004).

60. G. Benenti and G. Casati, G. Strini, *Principles of quantum computation and information*, (Singapore ; River Edge, NJ: World Scientific Pub., c2004).

61. J. Gruska, *Quantum computing*, (London: McGraw-Hill, 1999).

62. D. Bouwmeester, A. K. Ekert, A. Zeilinger, *The physics of quantum information : quantum cryptography, quantum teleportation, quantum computation*, (Berlin ; New York : Springer, c2000).

63. W.H. Zurek, Phys. Rev. D **24**, 1516 (1981).

64. W.H. Zurek, Phys. Rev. D **26**, 1862 (1982).

65. H.D. Zeh, Found. Phys. **169** (1970).

66 E. Joos, and H. D. Zheh, Z. Phys. B : Condens. Matter **59** 223 (1985).

67. D. Giulini, E. Joos, C. Kiefer, J. Kupsch, , I.-O. Stamatescuand, H.D. Zeh, *Decoherence and the Appearance of a Classical World in Quantum Theory*, (Springer, Berlin, 1996).

68. B. D'Espagnat, *Conceptual Foundations Of Quantum Mechanics*, (Perseus Books, c1999).

69. M. Schlosshauer, Rev. Mod. Phys. **76**, 1267 (2004).

70. D. Bohm, *Quantum theory*, New York, Prentice-Hall, 1951.

71. H. D. Zeh, (2002). *"Decoherence: Basic Concepts and Their Interpretation."* Draft for
second edition of Chapter 2 of "Decoherence and the Appearance of a Classical World in Quantum Theory" (D. Giulini et al., Springer 2003).

72. H. D. Zeh, Lect. Notes Phys. **538,** 19 (2000).

73. W. H. Zurek, Physics Today **44**, 36 (1991).

74. A. Peres, *Quantum theory: concepts and methods*, (Dordrecht; Boston : Kluwer Academic Publishers, c1995).

75. J. J. Sakurai, *Modern Quantum Mechanics*, (Addison-Wesley Pub. Co., c1994).

76. M. Namiki, *Decoherence and quantum measurements*, (Singapore ; River Edge, N.J. : World Scientific, c1997).

77. M. Borisovich, *Quantum measurements and decoherence : models and phenomenology,* (Dordrecht ; Boston: Kluwer Academic Publishers, c2000).

78. A. Einstein, B. Podolsky and N. Rosen, Phys. Rev. **47**, 777 (1935).

79. C. Lu, J. L. Cheng, M. W. Wu, and I. C. da Cunha Lima, Phys. Lett. A **365**, 501 (2007).

80. G. Balasubramanian, P. Neumann, D. Twitchen, M. Markham, R. Koleson, N. Mizuochi, J. Isoya, J. Achard, J. Beck, J. Tissler, V. Jacques, P. R. Hemmer, F. Jelezko, and J. Wrachtrup, Nature Materials **8**, 383 (2009).

81. S. Kummer, and T. J. Basche, Phys. Chem. **99**, 17078 (1995).

82. D. P. DiVincenzo, Fortschr. Phys. **48**, 771 (2000).

83. W.K. Wootters and W.H. Zurek, Nature **299**, 802 (1982).

84. D. Dieks, Phys. Lett. A, **92**, 271 (1982).

85. L. M. K. Vandersypen, M. Steffen, G. Breyta, C. S. Yannoni, M. H. Sherwood and I. L. Chuang, Nature **414** 883 (2001).

86. B. E. Kane, Nature **393**, 133 (1998).

87. D. Loss and D. P. DiVincenzo, Phys. Rev. A **57**, 120 (1998).

88. R Miller, T. E. Northup, K. M. Birnbaum, A. Boca, A. D. Boozer and H. J. Kimble, J. Phys. B: At. Mol. Opt. Phys. **38**, S551 (2005).

89. A. Steane, Appl. Phys. *B.* **64,** 623 (1997).

90. D. Kielpinski, C. Monroe and D. J. Wineland, Nature **417**, 709 (2002).

91. J. I. Cirac and P. Zoller, Phys. Rev. Lett. **74**, 4091 (1995).

92. G. K. Brennen, C. M. Caves, P. S. Jessen, and I. H. Deutsch, Phys. Rev. Lett. **82**, 1060 (1999).

93. V. Giovannetti, D. Vitali, P. Tombesi, and A. Ekert, Phys. Rev. A **62**, 032306 (2000).

94. K. Fujii *et al* J. Opt. B*:* Quantum Semiclass. Opt. **6,** 502 (2004).

95. A. Blais, R. Huang, A. Wallraff, S. M. Girvin, and R. J. Schoelkopf, Phys. Rev. A **69**, 062320 (2004).

96. Y. Makhlin, G. Scöhn and A. Shnirman, Nature **398**, 305 (1999).

97. Y. Makhlin, G. Schöhn and A. Shnirman. *Rev. Mod. Phys.* **73**, 357 (2001).

98. Y. Nakamura, A. Pashkin and J. S. Tsai *Nature* **398**, 786 (1999).

99. A. Y. Kitaev, Ann. Phys. 303, 2 (2003).

100. M. Freedman, M. Larsen, and Z. Wang, Comm. Math. Phys. **227**, 605 (2002).

101. E. Farhi, J. Goldstone, S. Gutmann, M. Sipser (2000). ArXiv:quant-ph/0001106v1.

102. R. Hughes et al., A Quantum Information Science and Technology Roadmap, version2.0, Report LA-UR-04-1778, Advanced Research and Development Activity (ARDA) (2004), http://qist.lanl.gov/.

103. W. Harneit, Phys. Rev. A **65**, 032322 (2002).

104. A. Ardavan, et al Phil. Trans. R. Soc. Lond. A, 361, 1473 (2003).

105. J. J. L. Morton, A. M. Tyryshkin, A. Ardavan, S. C. Benjamin; K. Porfyrakis, S. A. Lyon and G. A. D. Briggs, Nature Physics **2**, 40 (2006).

106. M. Feng and J. Twamley, Phys. Rev. A **70**, 032318 (2004).

107. J. J. L. Morton, *Electron spins in fullerenes as prospective qubits.* Ph.D. Thesis. Oxford University 2005.

108. L. Ge, B. Montanari, J. H. Jefferson, D. G. Pettifor, N. M. Harrison, and G. A. D. Briggs, Phys. Rev. B **77**, 235416 (2008).

109. S. Okada, Phys. Rev. B **72**, 153409 (2005).

110. X. Zeng, Q. Bia, G. Guob and H. E. Rudac, Phys. Lett. A **313**, 21 (2003).

111. C. Meyer, W. Harneit, B. Naydenov, K. Lips and A. Weidinger, Appl. Magn. Reson. **27**, 123 (2004).

112. J. Twamley, Phys. Rev. A 67, 052318 (2003).

113. W. Harneit, K. Huebener, B. Naydenov, S. Schaefer and M. Scheloske, Phys. Stat. Sol. b, **244**, 3879 (2007).

114. C. Ju, D. Suter, and J. Du, Phys. Rev. A, **75**, 012318 (2007).

115. Benjamin, S. C et al. J. Phys.: Condens. Matter, **18**, S867 (2006).

116. Ş. Erkoç, T. Uzer, *Atomic and Molecular Physics*, (World Scientific, Singapore, 1996).

117. G. D. Mahan, *Many Particle Physics*, (Kluwer Academic/Plenum publishers, 2000).

118. D. A. McQuarrie, *Quantum Chemistry*, (Sausalito, Calif.: University Science Books, c2008).

119. H. Haken, H. C. Wolf, *Molecular physics and elements of quantum chemistry : introduction to experiments and theory*, (Berlin ; New York : Springer, c2004).

120. J. E. House, *Fundamentals of quantum chemistry*, (San Diego, Calif. : Academic Press, c2004).

121. C. Møller, M. S. Plesset, Phys. Rev. **46**, 618 (1934).

122. S. F. Boys, Proc. Roy. Soc. (London) A **201**, 125 (1950).

123. J. A. Pople, J. S. Binkley, R. Seeger, Int. J. Quant. Chem. Symp. **10**, 1 (1976).

124. W. Kohn and, L. J. Sham Phys. Rev. **140**, 1133A (1965).

125. P. Hosenberg and L. J. Sham Phys. Rev. **136**, B864 (1964).

126. M. Born, J. R. Oppenheimer, Ann. Physik., **84**, 457 (1927).

127. J. C. Slater, Phys. Rev., **35**, 210 (1930).

128. W. J. Hehre, R. F. Stewart, J. A. Pople, J. Chem. Phys. **51**, 2657 (1969).

129. J. S. Binkley, J. A. Pople and W. J. Hehre, J. Amer. Chem. Soc. **102**, 939 (1980).

130. R. Ditchfield, W. J. Hehre, J. A. Pople, J. Chem. Phys. **54**, 724 (1971).

131. L. H. Thomas, Proc. Camb. Phil. Soc. **23**, 542 (1927).

132. E. Fermi, Rend. Accad. Lincei **6**, 602 (1927).

133. E. Fermi, Z. Phys. **48**, 73 (1928).

134. P. Hohenberg and W. Kohn, Phys. Rev. **136**, B864 (1964).

135. W. Khon and L. J. Sham, Phys. Rev. **140**, A1133(1965).

136. J. P. Perdew and A. Zunger Phys. Rev. B, **23**, 5048 (1981).

137. S. Goedecker, M. Teter and J. Hutter Phys. Rev. B, **54**, 1703 (1996).

138. S. H. Vosko, L. Wilk and M. Nusair Can. J. Phys. **58**, 1200 (1980).

140. A. D. Becke. Phys. Rev. A **38**, 3098 (1988).

141. J. Perdew, Electronic Structure of Solids, (ed. P. Ziesche and H. Eschrig) (Akademie Verlag, Berlin1991)

142. J. P. Perdew, Y. Wang Phys. Rev. B **33**, 8800 (1986).

143. A. D. Becke, Phys. Rev. A **38**, 3098 (1988).

144. A. D. Becke, J. Chem. Phys. **98**, 5648 (1993).

145. C. Lee, W. Yang and R. G. Parr, Phys. Rev. B **37**, 785 (1988).

146. J. R. Heath, S. C. O'Brien, Q. Zhang, Y. Liu, R. F. Curl, F. K. Tittel, R. E. Smalley, J. Am. Chem. Soc. **107**, 7779 (1985).

147. I. M. Mikhailovskij, E. V. Sadanov, T. I. Mazilova, V. A. Ksenofontov and O. A. Velicodnaja Phys. Rev. B **80**, 165404 (2009).

148. J. A. Driscoll and K. Varga Phys. Rev. B **80**, 245431 (2009).

149. L. Lacerda, A. Bianco, M. Prato and K. Kostarelos Adv. Drug Delivery Rev. **58**, 1460 (2006).

150. G. Pastorin, W. Wu, S. Wieckowski, J. P. Briand, K. Kostarelos, M. Prato and A. Bianco Chem. Commun. **11**, 1182 (2006).

151. W. Wu, S. Wieckowski, G. Pastorin, M. Benincasa, C. Klumpp, J. P. Briand, R. Gennaro, M. Prato and A. Bianco, Angew. Chem. Int. Ed. Engl. **44**, 6358 (2005).

152. K. L. Hur, S. Vishveshwara and C. Bena Phys. Rev. B **77**, 041406(R) (2008).

153. M. Kociak, A. Y. Kasumov, S.Guron, B. Reulet, I. I. Khodos, Y. B. Gorbatov, V. T. Volkov, L. Vaccarini and H. Bouchiat Phys. Rev. Lett. **86**, 2416 (2001).

154. A. Sdki, L. G. Caron and C. Bourbonnais Phys.Rev. B **65**, 140515(R) (2002).

155. X. Ren, Z. Liu, Struct. Chem. **16**, 567(2005).

156. J. L. Martins and N. Troullier, Phys. Rev. B **46**, 1766 (2002).

157. S. Okada, Phys. Rev. B **72**, 153409 (2005).

158. S. Hino, H. Takahashi, K. Iwasaki, K. Matsumoto, T. Miyazaki, S. Hasegawa, K. Kikuchi and Y. Achiba, Phys. Rev. Lett. **71**, 4261 (1993).

159. T. Kato, S. Suzuki, K. Kikuchi, Y. Achiba, J. Phys. Chem. **97**, 13425 (1993).

160. J. Lu, X. Zhangc, X. Zhaoc, S. Nagased and K. Kobayashi, Chem. Phys. Lett. **332**, 219 (2000).

161. M. Zhang, L. B. Harding, S. K. Gray and S. A. Rice, Phys. Chem. A, **112**, 5478 (2008).

162. M. Pavanello, A. F. Jalbout, B. Trzaskowski and L. Adamowicz, Chem. Phys. Lett. **442**, 339 (2007).

163. S. Peng, X. J. Li, Struct. Chem. **20**, No.5789 (2009).

164. K. Yamamoto, M. Saunders, A. Khong, R. James Cross, Jr., M. Grayson, M. L. Gross, A. F. Benedetto, and R. B. Weisman, J. Am. Chem. Soc. **121**, 1591 (1999).

165. Y. Kubozono, H. Maeda, Y. Takabayashi, K. Hiraoka, T. Nakai, S. Kashino, S. Emura, S. Ukita and T. Sogabe, J. Am. Chem. Soc. **118**, 6998 (1996).

166. T. Huang, J. Zhao, M. Feng, H. Petek, S. Yang and L. Dunsch, Phys. Rev. Lett. B **81**, 085434 (2010).

167. B. Cao, T. Wakahara, T. Tsuchiya, M. Kondo, Y. Maeda, G. M. A. Rahman, T. Akasaka, K. Kobayashi, S. Nagase and K. Yamamoto, J. Am. Chem. Soc. **126**, 9164 (2004).

168. S. Hino, M. Kato, D. Yoshimura, H. Moribe, H. Umemoto, Y. Ito, T. Sugai, H. Shinohara, M. Otani, Y. Yoshimoto and S. Okada, Phys. Rev. B **75**, 125418 (2007).

169. J. Lu, L. Ge, X. Zhang, X. Zhao, Mod. Phys. Lett. B **13**, 97 (1999).

170. J. Lu, Y. Zhouc, X. Zhang and X. Zhao, Chem. Phys. Lett. **352**, 8 (2002)

171. T. Ohtsuki, K. Masumoto, K. Ohno, Y. Maruyma, Y. Kawazoe, K. Sueki and K. Kikuchi, Phys. Rev. Lett. **77**, 3522 (1996).

172. W. L. Yang, Z. Y. Xu, H. Wei, M. Feng and D. Suter, Phys. Rev. A **81**, 032303 (2010).

173. S. Tth, D. Quintavalle, B. Nfrdi, L. Korecz, L. Forr and F. Simon, Phys. Rev. B **77**, 214409 (2008).

174. Z. G. Yu, Phys. Rev. B **77**, 205439 (2008).

175. F. Elste and C. Timm, Phys. Rev. B **71**, 155403 (2005).

176. M. Feng and J. Twamley, Phys. Rev. A **70**, 032318 (2004).

177. J. C. Greer, Chem. Phys. Lett. **326**, 567 (2000).

178. L. Ge, B. Montanari, J. H. Jefferson, D. G. Pettifor, N. M. Harrison and G. A. D. Briggs, Phys. Rev. B **77**, 235416 (2008).

179. G. W. Morley, B. J. Herbert, S. M. Lee, K. Porfyrakis, T. J. S. Dennis, D. Nguyen-Manh, R. Scipioni, J. van Tol, A. P. Horsfield, A. Ardavan, D. G. Pettifor, J. C. Green and G. A. D. Briggs, Nanotechnology **16**, 2469 (2005).

180. J. J. BelBruno, Fuller. Nanotub. Car. Nanostruc. **10**, 23 (2002).

181. S. Okada, Phys. Rev. B **72**, 153409 (2005).

182. X. Zeng, Q. Bia, G. Guob and H. E. Rudac, Phys. Lett. A **313**, 21 (2003).

183. S. C Benjamin et al. J. Phys.: Condens. Matter **18**, S867 (2006).

184. G. Burkard and D.Loss, Phys. Rev. B **59**, 2070 (1999).

185. F. Meier, J. Levy and D. Loss Phys. Rev. B **68**, 134417 (2003).

186. A. D. Becke, Phys. Rev. A **38**, 3098 (1988).

187. A. D. Becke, J. Chem. Phys. **98**, 5648 (1993).

188. C. Lee, W. Yang and R. G. Parr, Phys. Rev. B **37**, 785(1988).

189. R. Ditchfield, W. J. Hehre, J. A. Pople, J. Chem. Phys. **54**, 724 (1971).

190. Gaussian03, Revision D.01, M. J. Frisch, G. W. Trucks, H. B. Schlegel, G. E. Scuseria, M. A. Robb, J. R. Cheeseman, J. A. Montgomery, Jr., T. Vreven, K. N. Kudin, J. C. Burant, J. M. Millam, S. S. Iyengar, J. Tomasi, V. Barone, B. Mennucci, M. Cossi, G. Scalmani, N. Rega, G. A. Petersson, H. Nakatsuji, M. Hada, M. Ehara, K. Toyota, R. Fukuda, J. Hasegawa, M. Ishida, T. Nakajima, Y. Honda, O. Kitao, H. Nakai, M. Klene, X. Li, J. E. Knox, H. P. Hratchian, J. B. Cross, V. Bakken, C. Adamo, J. Jaramillo, R. Gomperts, R. E. Stratmann, O. Yazyev, A. J. Austin, R. Cammi, C. Pomelli, J. W. Ochterski, P. Y. Ayala, K. Morokuma, G. A. Voth, P. Salvador, J. J. Dannenberg, V. G. Zakrzewski, S. Dapprich, A. D. Daniels, M. C. Strain, O. Farkas, D. K. Malick, A. D. Rabuck, K. Raghavachari, J. B. Foresman, J. V. Ortiz, Q. Cui, A. G. Baboul, S. Clifford, J. Cioslowski, B. B. Stefanov, G. Liu, A. Liashenko, P. Piskorz, I. Komaromi, R. L. Martin, D. J. Fox, T. Keith, M. A. Al-Laham, C. Y. Peng, A. Nanayakkara, M. Challacombe, P. M. W. Gill, B. Johnson, W. Chen, M. W. Wong, C. Gonzalez and J. A. Pople, Gaussian, Inc., WallingfordCT,2004.

191. A. E. Reed, R. B. Weinstock, F. Weinhold, J. Chem. Phys. **83**, 735 (1985).

192. R. S. Mulliken, J. Chem. Phys. **23**, 1833 (1955).

193. U. Burkert, N. L. Allinger, Molecular Mechanics, ACS Monograph, 177, Washington D.C. 1982.

194. N. L. Allinger, J. Am. Chem. Soc. **99**, 8127 (1977).

195. C. C. J. Roothaan, Rev. Mod. Phys. **23**, 69 (1951).

196. A.Ardavan et al., Phil. Trans. R. Soc. Lond. A **361**, 1453 (2003).

197. A. Ardavan et al., Phil. Trans. R. Soc. Lond. A **361**, 1453 (2003).

198. W. Harneit, Phys. Rev. A **65**, 032322 (2002).

199. C. Meyer, W. Harneit, B. Naydenov, K. Lips and A. Weidinger, App. Magn. Reson. **27**, 123 (2004).

200. J. J. L. Morton, A. M. Tyryshkin, A. Ardavan, S. C. Benjamin, K. Porfyrakis, S. A. Lyon and G. A. D. Briggs, Nature Physics **2**, 40 (2006).

201. J. Twamley, Phys. Rev. A **67**, 052318 (2003).

202. W. Harneit, K. Huebener, B. Naydenov, S. Schaefer and M. Scheloske Phys. Stat. Sol. (b) **244**, 3879 (2007).

203. M. Mehring, W. Scherer and A. Weidinger, Phys. Rev. Lett. **93**, 206603 (2003).

204. C. Ju, D. Suter, and J. Du, Phys. Rev. A **75**, 012318 (2007).

205. M. Feng and J. Twamley, Phys. Rev. A **70**, 032318 (2004).

206. M. Busl, R. Snchez and G. Platero, Phys. Rev. B **81**, 121306(R) (2010).

207. E. Vernek, C. A. Bsser, G. B. Martins, E. V. Anda, N. Sandler and S. E. Ulloa, Phys. Rev. B **80**, 035119 (2009).

208. I. P. Gimenez, C. Hsieh, M. Korkusinski, and P. Hawrylak, Phys. Rev. B **79**, 205311 (2009).

209. T. Kostyrko and B. R. Bulka, Phys. Rev. B **79**, 075310 (2009).

210. D. Schrer, A. D. Greentree, L. Gaudreau, K. Eberl, L. C. L. Hollenberg, J. P. Kotthaus, and S. Ludwig, Phys. Rev. B **76**, 075306 (2007).

211. M. Korkusinski, I. P. Gimenez, P. Hawrylak, L. Gaudreau, S. A. Studenikin, and A. S. Sachrajda, Phys. Rev. B **75**, 115301 (2007).

212. J. Kempe and K. B. Whaley, Phys. Rev. A **65**, 052330 (2002).

213. V. Srinivasa and J. Levy, Phys. Rev. B **80**, 024414 (2009).

APPENDIX

The Mid-Level Quantum Computation Roadmap

QC Approach	The DiVincenzo Criteria						
	#1	#2	#3	#4	#5	#6	#7
NMR							
Trapped Ion							
Neutral Atom							
Cavity QED							
Optical							
Solid State							
Superconducting							
Unique Qubits	This field is so diverse that it is not feasible to label the criteria with the symbols.						

 = a potentially viable approach has achieved sufficiently proof of principle.

 = a potentially viable approach has been proposed, but there has not been sufficient proof of principle.

 = no viable approach is known.

The column numbers correspond to the following QC criteria:

#1. A scalable physical system with well-characterized qubits.

#2.The ability to initialize the state of the qubits to a simple fiducial state

#3. Long (relative) decoherence times, much longer than the gate-operation time.

#4. A universal set of quantum gates.

#5. A qubit-specific measurement capability.

#6. The ability to interconvert stationary and flying qubits.

#7. The ability to faithfully transmit flying qubits between specified locations.